UNIVERSITY **POLITEHNICA** OF BUCUREŞTI

Faculty of Chimical Engineering and Biotechnologies

Department of Inorganic Chemistry, Physical Chemistry and Electrochemistry

DOCTORAL CHEMISTRY OF APPLIED CHEMISTRY AND MATERIALS SCIENCE

CSUD Decision No..... from........

PhD THESIS SUMMARY

EVALUTION OF PROPERTIES FROM QUANTUM MECHANICAL CALCULATIONS FOR AZULENIC COMPOUNDS

EVALUARE DE PROPRIETĂȚI DIN CALCULE DE MECANICĂ CUÁNTICĂ PENTRU COMPUȘI AZULENICI

PhD student: Eng. Alina-Alexandra VASILE (CORBEI)

PhD COMMISION

President	Prof. Emerit Dr. Ing. Teodor VIȘAN	from	University Politehnica of Bucharest
PhD Supervisor	Prof. Emerit Dr. Ing. Eleonora-Mihaela UNGUREANU	from	University Politehnica of Bucharest
Reviewer	Prof. Emerit Dr. Ing. Olga IULIAN	from	University Politehnica of Bucharest
Reviewer	Prof. Dr. Ing. Farm. Gabriela STANCIU	from	University Ovidius Constanța
Reviewer	Dr. Ing. CS I Lucia PINTILIE	from	National Institute for Chemical-Pharmaceutical Research-Development, Bucharest

Bucharest
-2022-

CONTENT

INTRODUCTION

The constant need of chemists to understand complex phenomena and processes along with advances in information technology, have led to the development of a new branch of chemistry - *chemoinformatics*. It has strong implications for life sciences, such as molecular biology or biochemistry, with a major interest in medicine, pharmacy and the chemical industry. Its applications allow rational structural design and directing syntheses to obtain compounds or materials with improved properties. This discipline covers a wide range of topics, such as: applications of information technology in chemistry, involving the consultation and archiving of large libraries of compounds (small molecules and proteins containing structural properties and molecular descriptors, spectra, X-ray crystallography data, etc.), information processing, large-scale chemical data mining, computational tools for visualizing structures and interactions, computational models (for predicting interactions, calculating properties and bioactivity), molecular docking methodologies and dynamic simulations, virtual screening, modeling pharmacophores, fragment similarity analysis, estimation of ADMET properties (absorption, distribution, metabolism, excretion and toxicity), toxicity assessment, etc. These issues are common to areas of special interest, namely medical, pharmaceutical and chemical engineering whose main purpose is to improve the quality of life with applications in drug design, the development of new therapeutic strategies and new analytical tools (chemically modified electrodes). The stage of identification of new agents with potential in the fields of interest is preceded by the integration of the obtained chemical information, and their transformation involves mathematical models for the production, analysis and interpretation of statistical data.

This doctoral thesis addresses elements of chemoinformatics and is involved in the construction of databases for azulene compounds. The original studies involved consulting libraries of compounds (small molecules and proteins containing structural properties and molecular descriptors, spectra, X-ray crystallography data, etc.), processing information, using computational tools to visualize structures and interactions, and using models. advanced calculation tools for property prediction. The aim of these studies was the calculation of properties using quantum mechanics and the use of molecular docking methodologies. This goal was achieved using specialized calculation techniques and software programs for the silico characterization and preliminary evaluation of 1,3,4-thiadiazoles, for the evaluation of the properties of (Z) -5- (azulen-1-ylmethylene) -2- thioxothiazolidin-4-one and

azulene substituted with thiophene-vinyl-pyridine or furan-vinyl-pyridine, with further prospects for the synthesis of derivatives with improved properties (anticancer, with good absorption in the gastrointestinal and cerebral, etc.).

These aspects are common to fields of special interest (medicine, pharmacy and chemical engineering) and aim to improve the quality of life through their applications in drug design, development of new therapeutic strategies and development of new analytical tools (chemically modified electrodes).
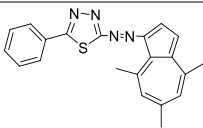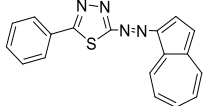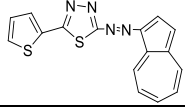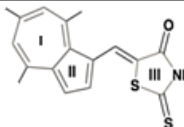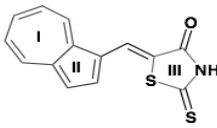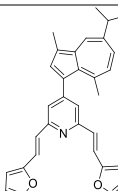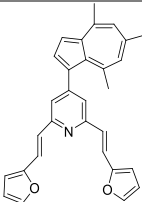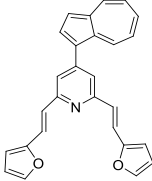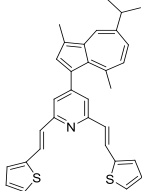
Compared to the experimental methods, the predictions obtained by these *in silico* working means contribute to: the reduction of the working time that is necessary for the realization of the laborious experimental analyzes, the reduction of the reagent acquisition costs. These *in silico* approaches are used for property predictions and have particularly important applications, such as the evaluation of drug similarity and the design of new therapeutic agents, the modeling of quantitative structure-activity relationships (QSARs).) and quantitative structure-property relationships (QSPRs), the prediction of oxidation-reduction potentials for molecular recognition in order to create new structures and make new predictions.
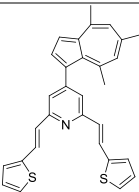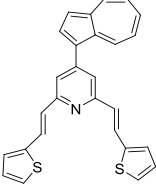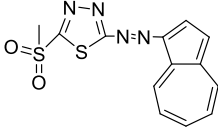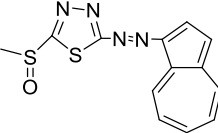
In recent years, new electrochemical methods have been developed that use sensors for detecting metals based on chemically modified electrodes. Within the *Laboratory of Electrochemical Processes in Organic Solvents (PESO)* from the University Politehnica of Bucharest (UPB), methods for the detection of heavy metals based on complexing electrodes modified with azulene were initiated and tested. This doctoral thesis is part of these concerns related to testing new ligands for the development of complexing electrodes. The thesis was developed in the *PESO* laboratory of the Department of Inorganic Chemistry, Physical Chemistry and Electrochemistry in the Faculty of Chemical Engineering and Biotechnology from University Politehnica of Bucharest and in collaboration with the National Institute for Chemical-Pharmaceutical Research-Development, Bucharest.

The thesis brings original contributions related to the evaluation of properties from quantum mechanics calculations for 14 azulene derivatives (**Table I.1**) synthesized in recent years in the *C. D. Nenițescu* Center for Organic Chemistry of the Romanian Academy in the Research Collective initiated by Dr. Alexandru C. Răzuș and coordinated by Dr. Liviu Bîrzan. In this thesis, 14 ligands were investigated, the properties of which were calculated using a dedicated software. The correlation with their experimental data from the specialized literature was performed. The results confirmed the ability of the tested ligands to complex heavy metal ions, in order to use them to obtain new sensors based on chemically modified electrodes. Using the chemoinformatics tools, the calculation of molecular properties and molecular descriptors was performed using two types of hybrid algorithms for 3 compounds, derivatives of 1,3,4-thiadiazole, and molecular docking simulations of these 3 investigated compounds on the *Human Topo IIα ATPase / AMP-PNP* target protein were performed, to see if they have the key physicochemical properties to identify them as good candidates for drugs. At the same time, oral bioavailability was assessed (capacity and time required for the active substance of a drug to be absorbed by the body).

This doctoral thesis presents studies evaluating the molecular properties and chemical reactivity parameters by quantum mechanical calculations for substituted and / or unsubstituted azulene-based compounds. These data were compared with the data obtained by experimental analyzes performed within the *PESO* laboratory team in order to validate the predictions obtained by using chemoinformatics tools with the experimental data.

Table I.1. The structures of the azulene derivatives investigated in the thesis

Crt. Nr.	Tipe of derivatives	Name of the compound	Structure	Results dissemination	
				Annex nr.	Number
1	1,3,4-thiadiazole	2-phenyl-5-((4,6,8-trimethylazulen-1-yl) diazenyl) -1,3,4-thiadiazole **(T1)**		Annex 1	Article 1
				Annex 2	Poster 5
2	1,3,4-thiadiazole	2- (azulen-1-yl) diazenyl) -5-phenyl-1,3,4-thiadiazole **(T2)**		Annex 1	Article 1
				Annex 2	Poster 5
3	1,3,4-thiadiazole	2- (azulen-1-yl) diazenyl) -5-(thiophen-2-yl) -1,3,4-thiadiazole **(T3)**		Annex 1	Article 1
				Annex 2	Poster 5
4	tioxotiazolidin-4-onă	(Z) -5 - ((5-isopropyl-3,8-dimethylazulen-1-yl) methylene) -2-thioxothiazolidin-4-one **(T1)**		Annex 1	Article 3
5	thioxothiazolidin-4-one	(Z) -5 - ((4,6,8-trimethylazulen-1-yl) methylene) -2-thioxothiazolidin-4-one **(T2)**		Annex 1	Article 3
6	thioxothiazolidin-4-one	(Z) -5 - [(azulen-1-ylmethylene] -2-thioxothiazolidin-4-one **(T3)**		Annex 1	Article 3
7	furan-vinyl-pyridine	2,6-bis ((E) -2- (furan-2-yl) vinyl) -4- (5-isopropyl-3,8-dimethylazulen-1-yl) pyridine **(O1)**		Annex 1	Article 4
				Annex 2	Poster 6
8	furan-vinyl-pyridine	2,6-bis ((E) -2- (furan-2-yl) vinyl) -4- (4,6,8-trimethylazulen-1-yl) pyridine **(O2)**		Annex 1	Article 4
9	furan-vinyl-pyridine	4- (azulen-1-yl) -2,6-bis ((e) -2-(furan-2-yl) vinyl) pyridine **(O3)**		Annex 1	Article 4
10	thiophene-vinyl-pyridine	2,6-bis ((E) -2- (thiophen-2-yl) vinyl) -4- (5-isopropyl-3,8-dimethylazulen-1-yl) pyridine **(S1)**		Annex 1	Article 2
				Annex 2	Poster 3

11	thiophene-vinyl-pyridine	2,6-bis ((E) -2- (thiophen-2-yl) vinyl) -4- (4,6,8-trimethylazulen-1-yl) pyridine **(S2)**		**Annex 1**	**Article 4**
12	thiophene-vinyl-pyridine	4- (azulen-1-yl) -2,6-bis ((e) -2- (thiophen-2-yl) vinyl) pyridine **(S3)**		**Annex 1**	**Article 4**
13	1,3,4-thiadiazole	2- (azulen-1-yldiazenyl) -5- (methylsulfonyl) -1,3,4-thiadiazole **(T4)**		**Annex 2**	**Poster 4**
14	1,3,4-thiadiazole	2- (azulen-1-yldiazenyl) -5- (methylsulfonyl) -1,3,4-thiadiazole **(T5)**		**Annex 2**	**Poster 4**

The doctoral thesis contains 7 chapters, and it is structured in two parts: LITERATURE REVIEW and PERSONAL CONTRIBUTIONS.

Part I, **LITERATURE REVIEW**, includes 3 chapters**:**

Chapter 1. Fields of application of chemoinformatics tools;

Chapter 2. Molecular docking as an instrument in the rational design of drugs;

Chapter 3. Molecular descriptors for evaluation of properties of some recognized organic compounds in therapy.

Part II, **PERSONAL CONTRIBUTIONS**, includes 4 chapters aimed at *in silico* characterizations aiming the evaluation of properties by quantum mechanical calculations for a series of azulene derivatives, with a view to their subsequent use in various fields, such as the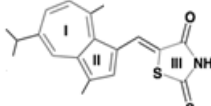 development of new analytical instruments (chemically modified electrodes for detection of heavy metal ions from water samples) or as potential candidates for drugs (3 chapters), namely:

Chapter 4. Calculation details;

Chapter 5. *In silico* characterization for preliminary evaluation of some azulenic 1,3,4-thiadiazoles

Chapter 6. Evaluation of the properties of some (z)-5-(azulen-1-ilmethylene)-2-thioxotiazolidin-4-ones using quantum mechanical calculations

Chapter 7. Evaluation of properties by quantum mechanical calculations for thiophen-vinyl-pyridine or furan-vinyl-pyridine substituted azulene

The doctoral thesis concludes with the general conclusions, the original contributions and the prospects for further development.

The best results obtained in the thesis were published in 3 scientific articles in ISI journals (*University Politehnica of Bucharest Scientific Bulletin. Series B, Symmetry*), and communicated at international and national scientific events (6 poster communications).

At the end of the thesis are attached the articles published during the doctoral thesis *in extenso*.

Chapter 4. Calculation details

4.1. Calculation details for *in silico* characterization and preliminary evaluation of 1,3,4-thiadiazoles azulenes

Molecular docking simulations were performed using *CLC Drug Discovery Workbench (Qiagen) Software on Human Topo IIα ATPase / AMP-PNP Target Protein Software* (PDB ID: 1ZXM) which contains as a co-factor a magnesium ion per chain, water and native ligand - co-crystallized phosphoaminophosphonic acid (ANP) adenylate ester at a resolution of 1.87 Å [1].

The structures of the ligands investigated were generated with *Spartan 16 Software*, Wavefunction Inc, USA [2], and optimized by simulations of molecular mechanics in force fields (MMFF) [3], which led to the establishment of conformations with the lowest energy to choose the most stable of all conformers. For example, **Figure 4.1** shows the chemical structure (a) and the geometry minimized with the arbitrary labeling of atoms chosen by the software (b) for one of the studied compounds, respectively **T1**, the representations for the other compounds (**T2**, **T3**, **T4**, **T5**) are made in the same way and are found in Chapter 5.2.

The water molecules and the existing co-factor (magnesium ion) were removed before docking. Co-crystallized phosphoaminophosphonic acid (ANP) adenylate ester is also called native or natural ligand. An attempt was made to reintegrate it into the complex by re-docking, this step being a method of validating the chosen docking protocol. Following this procedure, a docking position similar to that of the native ligand was obtained. Thus, the chosen docking protocol was validated. The A-chain binding pocket at 159.23 Å2 [4] was identified as the site where the native ligand interacts with the protein. The results are given according to the docking score (docking score) and as a mean square deviation (RMSD).

The property calculations were performed using the Functional Density Theory (DFT) with the *B3LYP* hybrid functional [5] with the set of polarization bases 6-31G * [6] for an equilibrium geometry in the ground state. Physico-chemical descriptors were calculated with *Spartan 16 Software*, Wavefunction Inc, USA [2] and the online platform SwissADME (http://www.swissadme.ch) [7]. The parameters from **Figures 4.2** and **4.3** were calculated for **T4** and **T5** compounds [8] using *Spartan 14 Software*, Wavefunction Inc, USA [2].

a. b.
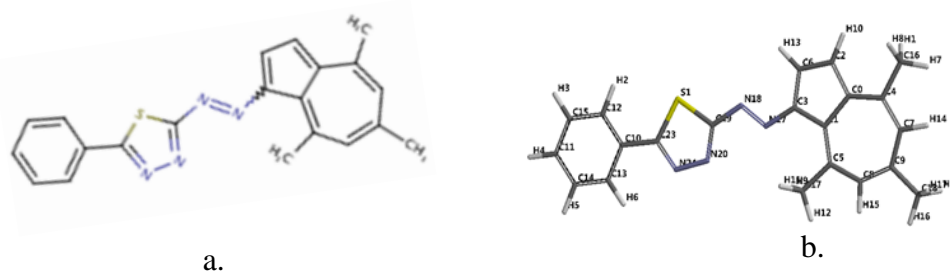
Figure 4.1. Chemical structures (a) and 2D optimized geometries / labeled (b) for the compound **T1** - ((azulen-1-yl) diazenyl) -1,3,4-thiadiazole obtained using *Spartan 14 Software.*

4.2. Calculation details when evaluating the properties of (Z)-5-(azulen-1-ylmethylene)-2-thioxothiazolidin-4-one

The calculations were carried out using Spartan 14 Software Wavefunction, Inc. Irvine CA, USA [2]. For the equilibrium geometry at ground state in a vacuum, a series of calculations of molecular properties and quantum chemical parameters was done using Density Functional Theory [10], software algorithm *B3LYP* method (the Becke's three parameter hybrid exchange functional with the Lee – Yang – Parr functional correlation [5] and polarization basis set 6-31G (d, p) [11] and *ωB97XD* / 6-311++G (d, p) density functional model, previously stated as an appreciable improvement

over other empirical dispersion corrected density functionals [12]. The ab initio calculation of NMR chemical shifts was achieved with a gauge including atomic orbitals (GIAO) [13]. The density functionals models employed by Spartan software used empirically corrected ^{13}C [14] chemical shifts to reduce the errors in comparison with uncorrected ones [15].

4.3. Calculation details when evaluating the properties of thiophenyl-vinyl-pyridine and furan-vinyl-pyridine substituted azulenes

The properties 'computations were realized with Spartan 14 software Wavefunction, Inc. Irvine CA, USA [2] for the lowest energy conformers of each structure, in vacuum conditions, at ground state using DFT models [10]. Two levels of theory *B3LYP* - the Becke's three-parameter hybrid exchange functional with the Lee–Yang–Parr correlation functional [5] with basis set 6-31G (d, p) [11, 16] and *ωB97XD* with basis set 6-31G (d, p) [12] were used. In this article [17] we use the notations *B3LYP* for *B3LYP* / 6-31G (d, p) and *ωB97XD* for *ωB97XD* / 6-31G (d, p).

For one compound, 2,6-bis ((E)-2-(furan-2-yl) vinyl) -4- (4,6,8-trimethylazulen-1-yl) pyridine (**O2**) substituted with furan-vinyl-pyridine is shown below in **Figure 4.4** molecular properties and QSAR [18] in using Spartan 14 Software, Wavefunction Inc, USA [2].

Selective bibliographic references Chapter 4
[4] **A.-A. Vasile (Corbei)**, A. Stefaniu, L. Pintilie, G. Stanciu, E.-M. Ungureanu, *In silico* characterization and preliminary anticancer assessment of some 1,3,4-thiadiazoles, U.P.B. Sci. Bull., 2021, B, 83, 3,
[8] **A.-A. Vasile (Corbei)**, V. Anastasoaie, M. Cristea, E.-M. Ungureanu, A. Stefaaniu, Theoretical studies using quantum mechanical calculaations for 1,3,4-thiadiazole derivatives with electrochemical applications, XXVI [th] International Symposium on Bioelectrochemistry and Bioenergetics of the Bioelectrochemical Society on Bioelectrochemistry for improved Life Quality, 9-13th May 2021, Cluj Napoca, Romania
[9] **A.-A. Vasile**, A. Stefaniu, O. Matica, E.-M. Ungureanu, Qunatum reactivity parameters computations for electrochemical behavior assesement, International symposium "The environment and the industry" E-SIMI 2020, September 24-25, 2020.
[15] **A.-A. Vasile (Corbei)**, E.-M. Ungureanu, G. Stanciu, M. Cristea, A. Stefaniu, Evaluation of (Z)–5-(Azulen-1-ylmethylene)-2-thioxothiazolidin-4ones Properties Using Quantum Mechanical Calculations, Symmetry, 2021,13, 1462.
[17] O. Ciocirlan, E.-M. Ungureanu, **A.-A. Vasile (Corbei)**, A. Stefaniu, Properties' Assessment by Quantum Mechanical Calculations for Azulenes Substituted with Thiophen- or Furan-vinyl-pyridine, Symmetry, 2022, 14, 354.
[18] **A.-A. Vasile**, G. Stanciu, E.-M. Ungureanu, A. Stefaniu, Global reactivity analysis from quantum parameters on 2,6-bis ((E)-2-(furan-2-yl)vinyl)-4-(4,6,8-trimethylaculen -1-yl)pyridine structure, IX International Scientific Conference Actual Problems of Solid State Physics, November 2021, Minsk, Belarus.

Chapter 5. *IN SILICO* CHARACTERIZATION AND PRELIMINARY ANTICANCER ASSESSMENT OF SOME 1,3,4-THIADIAZOLES

5.1. Docking studies performed on azulenic 1,3,4-thiadiazoles

The aim of this study was to evaluate the antiproliferative potential for three azulene derivatives of 1,3,4-thidiazole synthesized and characterized for the first time in the *CD Neniţescu* Center for Organic Chemistry of the Romanian Academy. The evaluation was performed by addressing molecular

docking during a doctoral internship conducted at the Institute for Chemical-Pharmaceutical Research-Development in Bucharest.

In this context, possible medical applications were established by accelerated *in silico* evaluation using computational tools to identify intra-molecular interactions and binding affinity of the *Human Topo IIα ATPase / AMP-PNP* target protein affinity (with the structure shown in **Figure 5.1**.) with thiadiazole ligands.

The target protein is known from numerous studies over the past few years and for its ability to prevent the proliferative process of tumors. Key bioavailability and key physicochemical properties were identified using dedicated software to identify the ability of ligands as drugs.

1,3,4-Thiadiazoles are aromatic heterocyclics containing nitrogen and sulfur atoms, known for their potential biological and pharmacological properties [1-3], which may be associated with structure. Several of their derivatives showed antimicrobial activity (eg 2-amino-1,3,4-thiadiazole) [4-7], anti-inflammatory [8], anticonvulsant [9,10], antituberculosis [11], or antiproliferative activity. [12, 13].

Starting from the concept of calculating the local scaffolds of analog series [14], this study turned its attention to 1,3,4 - thiadiazole derivatives, recently synthesized and characterized [15] for the evaluation of their antiproliferative potential. This has been done by tracking topoisomerase II in human DNA and other cancer-related targets and is an attractive approach for the design of new anticancer therapeutic agents [16].

5.2. Molecular docking protocol for azulenic 1,3,4-thiadiazoles

Molecular docking simulations were performed using *CLC Drug Discovery Workbench (Qiagen) Software* on *Human Topo IIα ATPase / AMP-PNP* target protein (PDB ID: 1ZXM) containing as co-factor magnesium ions, water and native ANP ligand to a resolution of 1.87 Å [17].

Structures of the ligands investigated 2-phenyl-5 - ((4,6,8-trimethylazulen-1-yl) diazenyl) - 1,3,4-thiadiazole (**T1**), 2- (azulen-1-yl) -5-phenyl -1,3,4-Thiadiazole (**T2**) and 2- (azulen-1-yldiazenyl) -5- (thiophen-2-yl) -1,3,4-thiadiazole (**T3**) were generated with *Spartan 16 Software*, Wavefunction Inc., USA [18] and optimized by molecular force field simulations (MMFF) [19] which led to the establishment of the lowest energy conformations, to choose the most stable of all conformations. The chemical structures are shown in **Figure 5.4**, and the minimized geometries with arbitrary atom labeling chosen by the software are found in **Figure 5.5**.

Co-crystallized phosphoaminophosphonic acid (ANP) adenylate ester is also called native or natural ligand. An attempt was made to reintegrate it into the complex by re-docking, this step being a method of validating the chosen docking protocol. Following this procedure, a docking position similar to that of the native ligand was obtained. Thus, the chosen docking protocol was validated. The binding pocket on the A chain at 159.23 Å^2 was identified as the site where the native ligand interacts with the protein. The results are given according to the docking score and the docking score as a mean square deviation (RMSD).

5.3. Molecular docking simulations for native ligand and synthesized azulenic 1,3,4-thiadiazole ligands

ANP was initially anchored in the crystal structure of *Human ATPase Topo IIα / AMP-PNP* (1ZXM) to validate the docking protocol and its interactions with the target protein were analyzed.

As shown in **Table 5.1.** and can be seen in **Figure 5.6**, the native ligand forms 21 interactions by hydrogen bonds (marked with dashed blue lines) with the amino acid residues in the A chain: LYS378, GLN376, ASN163, ARG162, GLY150, GLY161, ASN150, GLY150, GLY , TYR165, GLY166, GLU87, SER148, SER149, ASP94, THR147, LYS168, ALA167, ILE88, ILE141, PHE142, ILE141, PHE142, ILE217, ASN120, THR215, ILE125, GLY124, LYS123, AL A92, ASN95, ARG98.

Figure 5.7 shows the overlap of the ANP binding position, obtained by re-docking. As illustrated in **Figure 5.8**, it was found that all structures investigated have similar binding positions to

the native ligand, thus validating the docking methodology used. The binding pocket is shown as blue spheres in **Figure 5.9**.

T1

T2

T3
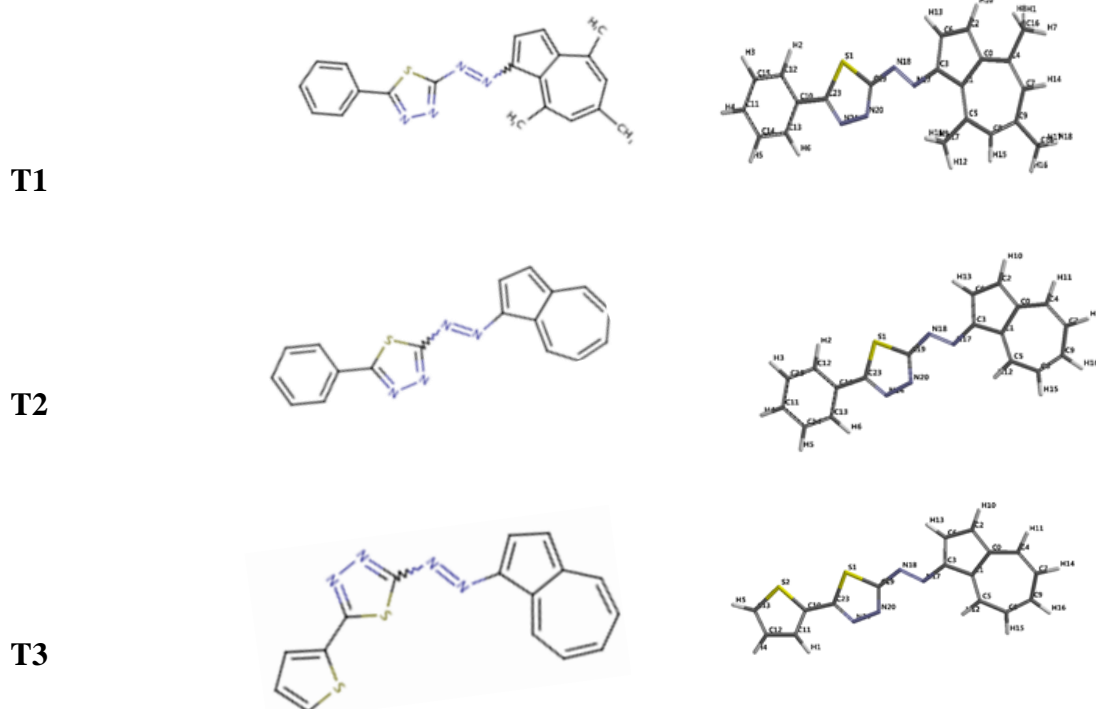
Figure 5.4. Chemical structures for compounds **T1, T2** and **T3** based on optimized equilibrium geometry obtained with *Spartan 16 Software*.

Figure 5.5. Representation of optimized geometries with arbitrary labeling chosen by *Spartan 16 Software* for **T1, T2** and **T3** compounds.

Table 5.1 shows that the co-crystallized ANP interacts through conventional hydrogen bonds through its many free hydroxyl orbitals Osp^3 attached to the tetrahydrofuran ring with SER149 and through its many Osp^2 orbitals of its phosphoaminophosphonic acid residue with ALA168, GL16, LY16, Y ASP91, SER148 ASN150, GLY164, TYR165, GLN376, ASN163, ARG162, LYS378. The nitrogen atom of the amino group (N6) in the purine derivative (adenine) forms a hydrogen bond with ASN150, and the nitrogen included in the phosphoaminophosphonic acid (N3B) group is involved in making three hydrogen bonds with the Nsp^2 atom in GLY164, ASN163 and ARG162. . The resulting docking score for ANP is -77.87 (RMSD = 0.82), suggesting a very close binding affinity and stability of the complex between ANP and DNA topoisomerase II and alpha isozyme.

As can be seen in **Table 5.2**, the ligands investigated interact poorly, forming two hydrogen bonds (**T1**) or three (**T2** and **T3**), with the remaining amino acid SER149. **T1** also interferes with the B chain via TYR34. The **T1** ligand interacts through the two nitrogen atoms of the azo bond that bind the azulene ring and thiadiazole (N17 and N18). **T2** forms three hydrogen bonds with SER149 and ASN150 through the two nitrogen atoms (N20 and N24) of the thiadiazole heterocycle. The docking simulations resulted in a lower score for **T2** (-58.26 compared to -61.42 for **T1**), although it apparently interacts more than the trimethyl-substituted azulene derivative. As for the **T3** compound, it forms hydrogen bonds with SER149 through the nitrogen azo bond near azulene (N17) and with LY**S1**57 through thiadiazole nitrogen, resulting in a docking score of -55.31. **Figures 5.10-5.12** illustrate intramolecular interactions in the complex resulting from DNA topoisomerase II - alpha isozyme and **T1**-**T3** investigated ligands.

Table 5.2. Results of docking simulations for **T1**-**T3** ligands on fragment *1ZXM*.

Target / Ligand Score/RMSD	Interacting group	Hydrogen bonds/Length (Å)
1ZXM / T1 -61.42 / 0.06	Chain A: PHE142, ILE125, ILE141, LYS168, ALA167, GLY166, ARG98, ASN91, ASN95, ASP94, THR159, GLN97, VAL158, LYS157, GLU155, ASN150, SER149, GLY164, SER148, THR147 Chain B: ILE33, TYR34	N17 sp^2 – O sp^3 SER149: A /2.561 N18 sp^2 – O sp^3 TYR34: B / 3.064
1ZXM / T2 -58.26 / 0.02	Chain A: ARG98, GLN97, ASN95, THR215, ASN120, ALA92, ASP94, ASN91, ILE217, THR159, VAL158, ALA167, PHE142, ILE141, ASN150, SER149, LYS157, ILE125	N20 sp^2 – N sp^2 ASN150/ 3.111 N20 sp^2 – O sp^3 SER149 / 2.762 N24 sp^2 – O sp^3 SER 149 / 3.015
1ZXM T3 -55.31 / 0.15	Chain A: THR147, SER149, SER148, ASN150, LYS157, VAL158, THR159, GLN97, ASP94, ASN91, ASN95, ALA167, ARG98, LYS168, PHE142, ILE141 Chain B: TYR34	N17 sp^2 – O sp^3 SER149 / 3.142 N20 sp^2 – O sp^3 SER149 / 2.578 N24 sp^2 – N sp^3 LYS157 / 3.078

Considering all above-mentioned findings, it can be assumed that, among the screened 1,3,4 thiadiazols derivatives, **T1** ligand exhibits the greater docking score, and consequently the stronger binding af-finity related with *Human Topo II ATPase*. It has higher antiprolifera-tive potency from the investigated ligands. Substituting the thiadiazol with a phenyl ring (**T2**) with a thiophen in position 5 (**T3**), leads to increased score (-58.26 vs -55.31). All these observations can be useful for further optimization, by designing hybrid structural analogues and enhancing the binding affinity by favor hydrophilic interactions.

Table 5.3. Descriptori moleculari calculați pentru predicția biodisponibilității orale (valorile care depășesc limitele stabilite pentru biodisponibilitatea orală sunt îngroșate).

Ligand	MW*	PSA*	TPSA*	HBD	HBA	logP	WLOGP	rb	RO5
ANP	**502.16**	-	311.36	5	**18**	-7.56	-2.37	8	2
T1	358.46	34.289	78.74	0	4	**5.24**	6.65	3	**1**
T2	316.38	36.099	78.74	0	4	**5.49**	5.73	3	**1**
T3	322.41	36.404	106.98	0	4	**5.21**	5.79	3	**1**

* Unități: MW – mol $\cdot$kg^{-1}; PSA and TPSA - Å^2

Lipinski C.A. et al. [23,24] established restrictions for molecular weight (MW $\leq$ 500 Da), number of hydrogen bond donors (HBD $\leq$5), number of hydrogen bond acceptor (HBA$\leq$10) and the octanol-water partition coefficient (logP $\leq$5) in order to evaluate the oral availability of drug candidates and to assess their pharmacokinetics. Veber and co-workers [25] added supplementary limitations for

polar surface area (PSA ≤140 Å^2) and flexibility of the molecules (no more than 10 rotatable bonds) to improve the predictions about drug-likeness.

In **Table 5.3**, are listed the key molecular descriptors, calculated to evaluated such properties of pharmacological interest: molecular mass (MW), polar surface area (PSA), calculated with *Spartan software*, TPSA – topological polar surface area, calculated with *SwissADME* online platform, counts of hydrogen-bond donors (HBD) and acceptors (HBA), the water-octanol partition coefficient calculated with *Spartan* (logP) and with *SwissADME* tools (WLOGP), number of rotatable bonds (rb) and number of Lipinski's rule of five violations (RO5). In *Spartan* procedures, logP is estimated according to the method of Ghose, Pritchett and Crippen, 1988 [26]. *SwissADME* tools uses the atomistic method implemented by Wildman S.A. and Crippen G.M., 1999 [27] to calculate logP (WLOPG). Topological surface area (TPSA) values are calculated from Ertl P. et al 2000 [28] method, with *SwissADME* prediction tools.

As observed form **Table 5.3**, the investigated 1,3,4-thiadiazols derivatives respect all properties restrictions, except logP, that is greater than 5, suggesting highly lipophilic behavior, with poor aqueous solubility. Generally, this parameter servs to categorization of the compounds by water-solubility and membrane-permeability; values of logP over 5 suggest poor absorption or permeation. This aspect can be improved by structure optimization of such ligands containing together azulene and thiadiazol moieties, to increase the hydrophilicity and to enhance their interacting capacity; thus, the possibility to become biologically active, can be successfully achieved. The co-crystallized ANP reveals 2 Lipinski's violations, due to its molecular mass, greater than 500 mol·kg^{-1} and to many hydrogen bond acceptors (18>10). Its structure is highly hydrophilic (negative logP value).

In drug design and development, an intuitive and rapid method to assess the passive gastrointestinal absorption and brain access of small is *the Brain Or IntestinaL EstimateD permeation method* (BOILED-Egg) by computing the lipophilicity and polarity [29]. **Figure 5.13** represents the plot of two physicochemical descriptors, WLOGP-*versus*-TPSA, as BOILED-Egg representation, allowing the evaluation of passive gastrointestinal absorption (HIA – Human Gastrointestinal Absorbtion) and brain penetration (BBB– Blood-Brain-Barrier Penetration) in function of the position of the molecules in the graph. **T2** is in the withe ellipse, indicating the probability to be passively absorbed by the gastrointestinal tract. **T1** and **T3** are represented in the grey zone, suggesting that these molecules are not well absorbed, not blood-brain barrier (BBB) permeant. **T1** (point colored in blue) is predicted to be substrate of the P-glycoprotein (PGP+) and hence actively pumped up from the brain or to the gastrointestinal lumen. **T2** and **T3** (points colored in red) are predicted as non-substrate of the P-glycoprotein (PGP-). Although very hydrophilic (WLOGP= -2.37), the native ligand, ANP is out of range in the *BOILED-Egg* plot, due to very high value of the polar surface area, greater than the maximal required value (311.36 >> 140 Å^2) **[30].**

5.4. Conclusions on docking simulations for native ligand and synthesized azulenic 1,3,4-thiadiazole ligands

An attempt to evaluate three hybrid compounds containing azulene and thiadiazole moieties coupled by azo bond in regard with their potential as drug candidates with anti-proliferative activity was made. Poor hydrophilicity of investigated molecules has as consequence the probability of poor or passive absorption the gastrointestinal tract. Also, the study leads to the conclusion that **T1** and **T3** are not blood-brain barrier permeant. Regarding molecular docking simula-tion lower docking score for the investigated structures than for the native ligand were observed. **T1** ligand exhibits the greater docking score and stronger binding affinity related with *Human Topo IIα ATPase*. All these finding constitute preliminary screening results, suggesting that forward structural optimization is mandatory, by add-ing hydrophilic groups such as hydroxyl, amino, sulphonyl, etc. in order to increase the hydrophilic-lipophilic balance. Optimized hybrid structural analogues with antiproliferative potency

can be designed starting from the results of this accelerated computational screening, for further pre-clinical assays [30].

5.5. Calculations of quantum mechanics on azulene 1,3,4-thiadiazole derivatives with electrochemical applications

Theoretical structural studies have been performed on other azulene derivatives: 2-(azulen-1-yldiazenyl)-5-(methylsulfonyl)-1,3,4-thiadiazole - **T4** and 2-(azulen-1-yldiazenyl)-5- (methyl-sulfinyl)-1,3,4-thiadiazole - **T5**, whose chemical structures are represented in **Figures 5.14-5.15**.

The calculation of the molecular properties and descriptors in **Table 5.4** was performed by quantum mechanical calculations using the DFT method, with *Spartan Software* [32], the *B3LYP* hybrid functional and the 6-31+ G (d, p) polarization base set [20].

The calculation resulted in detailed electronic properties and key molecular descriptors that were used to evaluate the potential utility of the compounds studied as ligands for the recognition of heavy metals. Starting from the values of the energies of the molecular orbitals HOMO and LUMO [15], the quantum reactivity parameters were calculated, whose values can be found in **Table 5.5**.
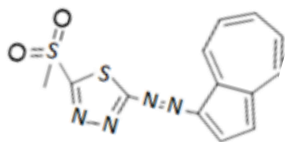
Figure 5.14. Chemical structure of compound **T4.**
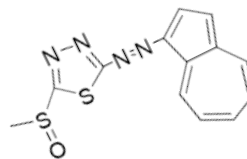
Figure 5.15. Chemical structure of compound **T5.**

Representations of electrostatic potential (EPM) maps (**Figure 5.16**) derived from the electrical charge distribution of the investigated structures and the diagram of frontier molecular orbitals (**Figure 5.17**) and are used to predict global reactivity [15, 33] and probable nucleophilic and electrophilic areas, respectively . On EPM representations the potential increases in the order: red <orange <yellow <green <blue. The color indicates the value of the electrostatic potential. The red spots suggest negative potentials observed on the sulfonyl and sulfinyl groups and on the N-N atoms of the thiadiazole ring, which is related to the most likely position for an electrophilic attack [31]. The blue color indicates potentially positive regions.

The Mulliken charges (**Figure 5.18**) and the hydrogen donor and acceptor centers (**Figure 5.19**) were calculated and a correlation was made between the experimental redox potentials [15] and the energies calculated for the frontier molecular orbitals (**Figure 5.20**) and a correlation was observed. very good linear [31].

The study, the results of which are presented in this Subchapter 5.5 [31], together with the results of the calculated quantum reactivity parameters provide valuable information for investigations into the potential application of these compounds in obtaining sensors for the recognition of heavy metal ions.

Chemical reactivity and kinetic stability for compounds **T4** and **T5** (data from the energy gap of frontier molecular orbitals) have similar values due to their similar structures. Their electronic properties related to charge distribution (dipole moment and polarizability) vary as follows: **T4**> **T5**, being correlated with the contribution of sulfonyl and sulfinyl groups to the polar surface area (PSA), which lead to variations in area and volume (**Table 5.4**) .
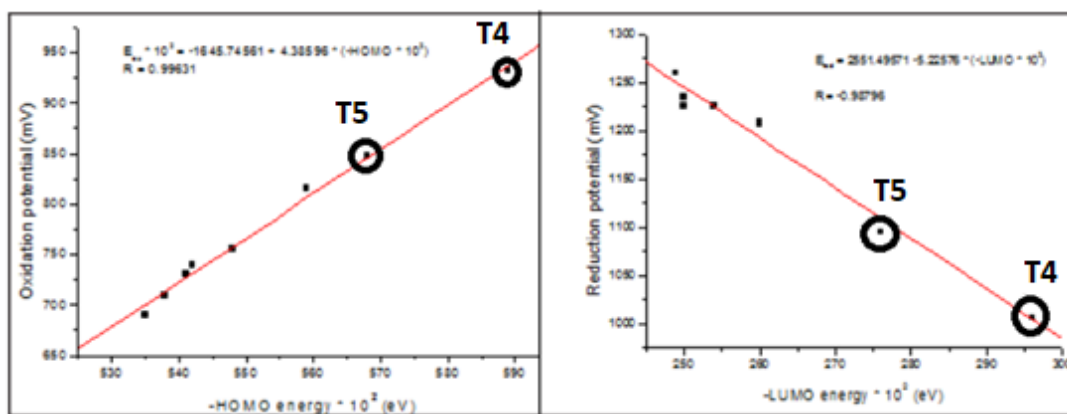
Figure 5.20. Correlation between experimental redox potentials and calculated energies for frontier molecular orbitals for **T4** and **T5** compounds [31].

Differences in the minimum values of the electrostatic potential (MinELPot - Minimum Electrostatic Potential) have been identified, the most negative value being located on the oxygen atoms of the sulfonyl and sulfinyl functional groups [31].

From the experimental electrochemical data [15], linear correlations were found (**Figure 5.20**) between the oxidation potential and the calculated HOMO energy and the reduction potential and the calculated LUMO energy (**Table 5.5**).

Local atomic charges (Mulliken population analysis - **Figure 5.18**) were assessed by calculations based on local electron density.

Selective bibliographic references Chapter 5

[30]. **A.-A. Vasile (Corbei)**, A. Ștefaniu, L. Pintilie, G. Stanciu, E.-M. Ungureanu, In silico characterization and preliminary anticancer assessment of some 1,3,4-thiadiazoles, U.P.B. Sci. Bull., 2021, B, 83, 3,.

[31] **A.-A. Vasile (Corbei)**, V. Anastasoaie, E.-M. Ungureanu, A. Ștefaniu, Theoretical Studies Using Quantum Mechanical Calculations for 1,3,4-Thiadiazole Derivatives with Electrochemical Applications, XXVIth Intrenational Symposiun on Bioelectrochemistry and Bioenergetics BES (online), 9–13 Mai 2021, Cluj-Napoca, ROMANIA, Poster **S2**-P017.

Chapter 6. Evaluation of (Z)-5-(Azulen-1-ylmethylene)-2-thioxo-thiazolidin-4-ones properties using quantum mechanical calculations

6.1. Properties of (Z)-5-(Azulen-1-ylmethylene)-2-thioxothiazolidin-4-ones

Previous studies performed in the Laboratory of Electrochemical *Processes in Organic Solvents (PESO)* at the University Politehnica of Bucharest correlated electrochemical properties for different organic compounds with structural parameters using calculations performed by DFT to make a rational design for new materials with improved electrochemical properties [1-8].They are based on the link between the energy levels corresponding to the highest occupied molecular orbital (HOMO) or the lowest unoccupied molecular orbital (LUMO) and the electrochemical oxidation and reduction potentials, respectively [9–11]. Strong linear correlations of DFT-calculated HOMO/LUMO energies using *B3LYP* /6-31G(d) functional [12,13] and experimental redox potentials were found for polycyclic aromatic hydrocarbons by D. Méndez-Hernández and co-workers [14], highlighting the idea that quick, accurate and low-cost predictions using the *B3LYP* /6-31G(d) functional represent a reliable approach to apply on other molecules to evaluate their electrochemical properties. A comparative computational study using different density functionals on small neutral molecules, at ground state, has recently

shown that the use of the *ωB97XD* model gives better performance for atomization energies and bond lengths predictions than commonly used *B3LYP* level of theory [15].

Such computer-aided approaches are very good alternatives for laborious investigations. The *PESO* research team is concerned with the choice of a specific ligand for building complexing modified electrodes which can be used as sensors for a specific target. The main interest in the present study was to find several parameters which characterize the best ligand among three (Z)-5-(azulen-1-ylmethylene)-2-thioxothiazolidin-4-one derivatives which were used for a specific modification of a glassy carbon electrode in view of obtaining selective recognition of HMs ions. These derivatives were reported as HMs ligands in heterogeneous systems based on chemically modified electrodes (CMEs). Their ability to coordinate HMs ions has recently been shown to be very selective [16]. DFT calculations were performed to provide accurate structural details and prediction properties in-silico approach, aiming to be correlated with the electrochemical behaviour and other properties of investigated ligands. Previously published data reveal that among other monomers (pyrrole, thiophene, etc.), azulene shows low ionization energy, high electron mobility and less symmetric structure, due to its polarized structure formed by fusing a seven-membered ring with a five-membered ring of carbon atoms. This makes azulene a very interesting building block for the synthesis of new advanced materials [17–20].

The structures of investigated compounds are shown in **Figure 6.1.** In order to depict the structural differences, the common parts of their structures were similarly colored in: red—the seven-membered azulene ring (I), blue—the five-membered azulene ring (II), and green—the cycle of the thiazolidine (III).
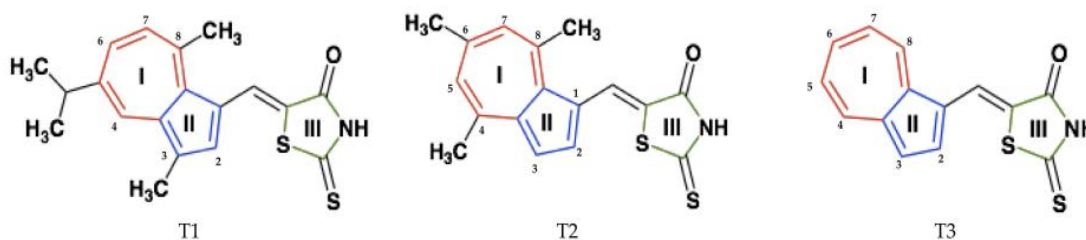
Figure 6.1. Structure of investigated compouns **T1-T3.**

The investigated ligand structures contain a part of rhodanine (III), known for its HMs complexing properties [21]. Azulene derivatives of rhodanine can be used in the precise determination of metals, in the same way that *p*-dimethylaminophenylenrhodanine was used for the precise determination of Cu, Ni, Fe and Zn ions [22], or in the same way that triarylamine rhodanine derivatives were used as colorimetric sensors for the detection of Ag (I) and Hg (II) ions [23].

The second distinct part of the investigated ligand structures in **Figure 6.1** is an azulene moiety substituted by different alkyl groups (methyl = Me, *i*-propyl = *i*Pr): 3,8-Me$_2$-5-*i*Pr (**T1**), 4,6,8-Me$_3$ (**T2**), or unsubstituted (**T3**). This azulene part can serve as polymerizable unit to obtain modified electrodes.

The alkyl groups induce a +*I* effect and increase the electron densities of the molecules. Consequently, the alkyl-substituted compounds are expected to be easier oxidized and harder to be reduced than pattern compounds (**T3**). However, the steric effect of these groups makes the reductions more difficult to anticipate.

The azulene system is more stable when it is symmetrically substituted, but becomes very reactive by unsymmetrical substitution when the symmetry of the aromatic system is disrupted by the difference in the alkyl groups electronic influence. Therefore, it is expected that **T1 -** unsymmetrically substituted will react faster than **T2 -** symmetrically substituted with 4,6,8-Me$_3$ despite its higher volume.

Previous studies have highlighted the capacity of azulenes to be immobilized on electrodes through electropolymerization processes if 1,3 positions are free [24], or by π-stacking [25]. For sensor

applications, this last way is more advantageous [25], because the number of grafted complexing units on the electrode surface is increased, leading to a better response.

T1, **T2**, and **T3** ligands have push–pull structures that can be used to build modified electrodes with complexing properties. These compounds were electrochemically characterized, and their metal-binding properties were reported [16]. Even if their structures are quite similar, different complexing abilities have been found for the modified electrodes based on them. These experimental results led us to look for structural reasons to explain why the behaviour is so different. The results of DFT calculations are reported here and several calculated properties were compared with the experimental ones. Connections were made with the experimental results obtained in the use of the modified electrodes based on these compounds in HM analysis. **Table 6.1** gives several properties of **T1**–**T3**, and the experimental features which were found to be different in their use in the modified electrodes preparation/characterization, and utilization to analyze HMs ions from aqueous solutions.

Table 6.1. Experimental parameters related to ligand properties (lines 1–4), film formation (lines 5, 6), HMs analysis and detection limits (DLs) for metal ions (lines 7–11) for **T1**–**T3** ligands.

Crt. Nr.	Ligand	T1	T2	T3
1	**Ligand property** [Reference]	[45]	[40]	[46]
2	*Ea1* (V) from DPV 0.5 mM	**0.373 V**	0.473 V	0.541 V
3	Ec1 (V) from DPV 0.5 mM	-1.543 V	-1.541	-1.528 V
4	Solubility	~ 1 mM	~ 2 mM	~1 mM
5	**Film formation** [Reference]	Yes, for [**T1**] = 0.5 mM [45]	Yes, for [**T2**] = 0.5 mM [40]	Yes, for [**T3**] = 0.25 mM [40]
6	**Ferrocene redox probe** on CMEs *vs* bare electrode (conditions of preparation) [Reference]	Small decrese in the ferrocene peaks currents (EPC, succesive CV scanning, 0.5 mM) [45]	Noticeable decrease in the ferrocene peaks currents(EPC, succesive CV scannings, 0.5 mM) [40]	Noticeable decrease in the ferrocene peaks currents(EPC, succesive CV scannings, 0.25 mM) [46] - Small decrese in the ferrocene peaks currents (scanning, 1 mM) [35]
7	**HMs analysis*** [Reference]	Quite high DLs [45]	Medium DLs [40]	Lowest DLs [35]
8	DL_{Pb} (M)	10^{-6}	10^{-7}	**10^{-8}**
9	DL_{Cd} (M)	10^{-6}	10^{-7}	**$8 \cdot 10^{-8}$**
10	DL_{Cu} (M)	10^{-6}	**$5 \cdot 10^{-7}$**	$6 \cdot 10^{-7}$
11	DL_{Hg} (M)	10^{-4}	**$5 \cdot 10^{-7}$**	$6 \cdot 10^{-7}$

*DLs - limits of detection for HMs ions – the obtain values are smaller than the marked ones (lines 8-11).

The monomers (mainly characterized in **Table 6.1**, lines 1–4) were successfully deposited on glassy carbon electrodes through direct electropolymerization at anodic potentials in millimolar solutions of each ligand. The CMEs were tested then in ferrocene solutions in acetonitrile containing

0.1 M tetrabutylammonium perchlorate (TBAP) as supporting electrolyte (**Table 6.1**, lines 5 and 6). The films formations occurred in different ranges of monomer concentrations (line 5). Changes of the ferrocene redox signal of different amplitudes were found (line 6). These materials were tested vs. HMs (**Table 6.1**, lines 7–11). They were able to complex HMs ions from aqueous solutions [21,27], but the parameters for their analysis were very different (line 7). **T1**-modified electrodes have quite high detection limits (10^{-6} M for Pb, Cd, Cu and 10^{-4} M for Hg). **T2**-modified electrodes showed an intermediate behaviour, and their detection limits are of about 10^{-7} M. **T3**- modified electrodes showed the highest complexing ability leading to attractive values for the lowest detection limits (for instance DLPb $< 10^{-8}$ M).

Lines 5 and 6 in **Table 6.1** collect the characteristics of the film formation and characterization. It is expected that the electrochemical polymerization of azulene ligands on the electrode surface is intensified by the presence of alkyl groups, grafted on the azulene moiety (these effects are seen in the values of first oxidation potential *Ea1*- line 2 from **Table 6.1**). However, **T1** hardly formed films, while **T3** easily formed films. **T2** showed intermediate behaviour. The film formation ability seems to be in accord with the analytical performance [17,28], which is bigger for **T3** (lines 8-11)**.**

It is difficult to explain/predict the behaviour only from the analysis of the inductive effects of the substituents on the studied structures [29], because the investigated facts are quite complex involving several processes, as seen in **Table 6.1** (ligand polymerization, CME complexation, etc.). However, the ligand structure is decisive in all these steps, and the rationalization of these structural effects based on quantum mechanical calculations is found as a favorable approach. Similar calculations for other structures are of great use in reducing the number of experiments, which has a major economic impact in finding a way to anticipate the optimal structures.

6.3. Rezults of calculated properties

The first step in the calculation was to generate the 3D structures of the (Z) -5- (azulen-1-ylmethylene)-2-thioxothiazolidin-4-one derivatives and optimize their geometry optimization. This step aimed to establish the most stable conformer of each derivative, which has the minimum energy among its conformers. The atomic numbering schemes for the optimized geometries of the analyzed structures are arbitrarily assigned by Spartan 14 Software. The bond lengths calculated in the ground state and the angles as well as the predicted dihedral angles for the studied structures confirm the electronic effects of alkyl substituents on the structure of azulenes for optimized conformations of **T1-T3** molecules. Calculations were made for each structure for compliance with the lowest energy.

6.3.1. Predicted and experimental NMR chemical shifts

The *ab initio* calculation of ^{1}H- and ^{13}C-NMR chemical shifts was achieved. Correlations between predicted and experimental (found in [29]) chemical shifts for **T1–T3** were performed to check the prediction's accuracy for the investigated structures. They are listed in **Tables 6.2–6.7**. The structures of each compound were introduced in the table's heads using different notations that came from the computational algorithm generated by the software (denoted A1, A2, A3) and from the experimental data [29], according to IUPAC notations (denoted B1, B2, B3) to be in correspondence.

6.3.2. Molecular and QSAR propeties

Table 6.8 lists the results of DFT computations, describing molecular and quantitative structure–activity relationships (QSAR) properties of the investigated ligands using *B3LYP* /6-31G (d, p) and *ωB97XD/*6-311++G (d, p) density functional models.

The first seven lines of **Table 6.8** display the calculated molecular properties: molecular weight (line 1), (total) energy (line 2), aqueous solvation energy (Energy (aq) (line 3)), solvation energy (line 4), dipole moment (line 5), energy of the HOMO orbital (line 6), energy of the LUMO orbital (line 7). Lines 8-16 display QSAR properties: area (line 8), volume (line 9), polar surface area (PSA) (line 10), degree of deviation from perfect spherical shape molecule (ovality index) (line 11),

polarizability (line 12), rate of distribution between hydrophilic and hydrophobic media - the octanol - water partition coefficient (LogP) (13), count of hydrogen bond acceptor (HBA) (14) and donor (HBD) (15), minimum value of electrostatic potential (MinElPot) (16).

Table 6.8. Predicted molecular (lines 1–7) and QSAR (lines 8–16) properties of **T1**–**T3** calculated using *B3LYP* /6-31G (d, p) and *ωB97XD*/6-311++G (d, p) density functional models, respectively.

Crt. Nr.	Compound \ Parameter	Method	T1 $C_{19}H_{19}NOS2$	T2 $C_{17}H_{15}NOS2$	T3 $C_{14}H_9NOS2$
1	Molecular weight (g·mol^{-1})		341.50	313.45	271.36
2	Energy (au)	*B3LYP*	- 1661.81	-1583.18	- 1465.24
		ωB97XD	- 1661.74	-1583.12	- 1465.18
3	Energy (aq)	*B3LYP*	- 1661.83	- 1583.21	- 1465.27
		ωB97XD	- 1661.76	- 1583.14	- 1465.20
4	Solvatation Energy (kJ·mol^{-1})	*B3LYP*	- 54.10	- 57.65	- 61.34
		ωB97XD	- 51.67	- 55.18	- 59.49
5	**Dipole moment** (D)	*B3LYP*	9.04	8.87	7.83
		ωB97XD	8.48	8.25	7.56
6	*E* HOMO (eV)	*B3LYP*	-5.51	-5.33	-5.48
		ωB97XD	-7.13	-7.33	-7.44
7	*E* LUMO (eV)	*B3LYP*	-2.42	-2.42	-2.59
		ωB97XD	-1.04	-1.03	-1.22
8	Area (Å^2)	*B3LYP*	358.61	319.24	268.07
		ωB97XD	356.23	317.64	266.35
9	Volume (Å^3)	*B3LYP*	344.19	307.28	254.25
		ωB97XD	342.27	305.61	252.85
10	PSA (Å^2)	*B3LYP*	26.12	26.14	26.16
		ωB97XD	26.01	26.03	26.00
11	**Ovality index**	*B3LYP*	1.51	1.45	1.38
		ωB97XD	1.51	1.45	1.38
12	**Polarizability** (10^{-30} m^3)	*B3LYP*	68.63	65.61	61.32
		ωB97XD	67.70	64.68	60.41
13	**LogP**	*B3LYP*	2.56	1.81	1.29
		ωB97XD	2.56	1.81	1.29
14	HBD Count	*B3LYP*	1	1	1
		ωB97XD	1	1	1
15	HBA Count	*B3LYP*	4	4	4
		ωB97XD	4	4	4
16	**MinElPot** (kJ·mol^{-1})	*B3LYP*	-165.93	-163.84	-158.04
		ωB97XD	-170.10	-167.14	-162.72

The frontier molecular orbitals density distribution obtained by calculation for the studied structures is shown in **Figure 6.2**, along with the energy diagram and the gaps between the HOMO and LUMO *(ΔE)*. They were calculated using the *ωB97XD*/6-311++G (d, p) density functional model. For *B3LYP* /6-31G (d, p) model.

Starting from E$_{HOMO}$ and E$_{LUMO}$ energies given in **Table 6.8**, other related quantum descriptors resulted. **Table 6.9** gives the formulas and calculated values for: energy gap (ΔE), ionization potential (*I*), electron affinity (*A*), electronegativity (χ), global hardness (η), global softness (σ) [37,38], and global electrophilicity index (ω) [39] using *B3LYP* /6-31G (d, p) and *ωB97XD*/6-311++G (d, p) density

functional models. *I* and *A* were calculated by applying relationships proposed by Koopmans [40,41], respectively. The softness (σ) and hardness (η) descriptors derived from Pearson's Hard and Soft Acids and Bases Principle (HSAB) [42] and Maximum Hardness Principle (MHP) [43] describe the electronic reactivity, and the response to electronic perturbations, respectively [44]. The global electrophilicity index (ω), as defined by Parr R.G and co-workers [39], is a measure of the reactivity of chemical species in different environments (solvent or biological systems).

The electrostatic potential maps (EPM) are shown in **Figure 6.3**. The color indicates the value of the electrostatic potential. Red areas suggest negative potentials, color toward blue designate regions of positive potential. The potential increases in the order: red < orange < yellow < green < blue. Red regions suggest the potential sites for HMs ions complexation, where positive charges are most susceptible to be attracted.

Figure 6.4 gives the maps of local ionization potential obtained using *ωB97XD* /6- 311++G (d, p) density functional model. They reveal the regions from which electrons are most easily removed indicating the most susceptible sites to electrophilic attack.

In LUMO maps representation in **Figure 6.5**, the absolute value of LUMO is mapped onto an electron density surface (blue color for large values of LUMO and red color for small values), allowing to anticipate regions subjected to nucleophilic reactivity.

Table 6.9. Quantum chemical reactivity parameters (in eV) of **T1**–**T3** obtained using *B3LYP* /6-31G (d, p) and *ωB97XD*/6-311++G (d, p) density functional models.

Crt. Nr.	Ligand \ Parameter	T1		T2		T3	
		B3LYP	*ωB97XD*	*B3LYP*	*ωB97XD*	*B3LYP*	*ωB97XD*
1	$I = - E_{HOMO}$	5.21	7.13	5.33	7.33	5.48	7.44
2	$A = - E_{LUMO}$	2.42	1.04	2.42	1.03	2.59	1.22
3	ΔE (eV) $= I - A$	2.79	6.09	2.91	6.30	2.89	6.22
4	$\chi = (I + A)/2$	3.81	4.08	3.88	4.18	4.03	4.33
5	$\eta = (I - A)/2$	1.40	3.04	1.45	3.15	1.44	3.11
6	$\sigma = 1 / \eta$	0.71	0.33	0.69	0.32	0.69	0.32
7	$\omega = \mu^2 / 2\eta$	5.18	2.74	5.19	2.77	5.64	3.01

* Graphs based on electron density, obtained from quantum chemical calculations, using the functional level *ωB97XD* / 6-311 ++ G (d, p) are shown in **Figures 6.3-6.5**.

6.3.3. Correlation between DFT-calculated frontier molecular orbital's energies and experimental data

The calculated HOMO and LUMO energies (**Table 6.8** lines 6 and 7, respectively) were plotted against experimental oxidation and reduction potentials (**Table 6.1**, lines 2 and 3, respectively). Linear relationships obtained for reduction and oxidation potentials, and their corresponding equations, are given in **Table 6.10**, using either *B3LYP* or *ωB97XD* hybrid functions.

Table 6.10. Linear relationships obtained for oxidation and reduction potentials of investigated ligands and their correlation coefficient (R^2) for calculations with *B3LYP or ωB97XD functions. B3LYP (*a)* și (*b)*.

*y = a + b*x*	Funcțional	a	B	R^2
Potențial de oxidare (y în V) *vs*	*B3LYP*	-2.823	0.615	0.940
E_{HOMO} (x în eV)	*ωB97XD*	-3.457	0.537	0.994
Potențial de reducere (y în V) *vs*	*B3LYP*	-1.741	0.082	0.970
E_{LUMO} (x în eV)	*ωB97XD*	-1.620	0.075	0.943

6.4. Discussions about calculated predictions

6.4.1. NMR predictions

The *ab initio* calculation of NMR chemical shifts listed in **Tables 6.2–6.7** shows reasonably good results for predicted data in comparison with the experimental ones (taken from [29]). Good agreement between experimental and calculated data concerning ^{1}H-NMR and ^{13}C-NMR for **T1–T3** structures, except for H4 atom (the hydrogen from -NH of the cycle III) is found. The observed gaps are explained by the proton enolization due to the intermolecular proton transfers from -NH (-SH or -OH). Additionally, small deviations from experimental shifts can occur due to the presence of solvent [66].

6.4.2. Molecular and QSAR properties predictions

6.4.2.1. Highlighting results by using different functional models

The calculated values given in **Table 6.8** predicted by *B3LYP* /6-31G (d, p) and *ωB97XD*/6-311++(d, p) are quite similar for energy (line 2), energy (aq) (line 3), solvation energy (line 4), area (line 8), volume (line 9), PSA (line 10). The values are equal for ovality index (line 11), LogP (line 12), HBD Count (line 14), HBA Count (line 15). Identical values in terms of HBD and HBA counts are due to the existence of the same 2-thioxothiazolidinone complexing unit. The main differences between methods are seen in the dipole moment (line 5), EHOMO (line 6), ELUMO (line 7), polarizability (line 12), and MinElPot (line 16). However, both models lead to values that increase or decrease in the order **T1** > **T2** > **T3**, being correlated with the structure, as forward.

6.4.2.2. Highlighting variation of properties among investigated structures

By examining the values of the properties given in **Table 6.8** and taking into account the changes in the compound's structures, the main differences in magnitude are for the calculated dipole moment (line 5), ovality index (line 11), polarizability (line 12), LogP (line 12), and minimum electrostatic potential values (line 16). The dipole moment and the polarizability decrease in magnitude as expected, ranging in the order: **T1** > **T2** > **T3**. It is higher for the structure having more alkyl substituents. The ovality index varies in the same order, as the linearity of structures decreases with substitution, being related to molecular surface (line 8) and van der Waals volumes (line 9) which also decrease in the same order. The partition coefficient LogP is the parameter that varies the most for these structures in the same order. The obtained values suggest a hydrophobic character of the structures and confirm their low aqueous solubility (**Table 6.1**, line 4), especially for the ligands substituted with iso-propyl and methyl groups (**T3** and **T2**). However, logP values are not so high due to the contribution of the rhodanine moiety. This moiety is favorable for the complexing properties of all ligands, and also for the CMEs based on such ligands. LogP values could be related to the complexing property which was found for CMEs (**Table 6.1**, line 7). The best values are obtained for CMEs based on **T3**. MinElPot calculated form *ωB97XD* method for the investigated structures decreases in absolute values in the same order. More comments about this parameter are given forward, connected with the discussion of **Figure 6.3**.

The other related quantum descriptors for the studied structures resulted in **Table 6.8** such as energy (line 2) in absolute value, energy aq. (line 3) in absolute value, solvation energy (line 4), area (line 8) and volume (line 9), decrease in the order: **T1** > **T2** > **T3**, as expected, according to their molecular weight and azulene substituents (methyl and isopropyl). PSA (line 10) value presents insignificant variance for the three investigated structures, suggesting there is no distinction caused by polar substituents or significant disturbing electron distribution grafted on the skeleton. The major contribution in the polar character of the compounds is given by polar functional groups or atoms which are the heteroatoms present in their same complexing unit (the rhodanine). Consequently, PSA is quite similar for the investigated compounds. It is not significantly influenced by the methyl and isopropyl substituents of the azulene moiety, as shown by *B3LYP* /6-31G (d, p) calculation. However, the values

calculated by the *ωB97XD*/6-311++(d, p) model are higher for **T1** and **T2** than **T3**, putting in evidence the effect of the alkyl groups on the structure, and confirming the last model is better.

From **Figure 6.2**, a quite similar distribution of the frontier molecular orbitals can be observed for the three compounds. The frontier orbitals gap (ΔE) which characterizes the chemical reactivity of each molecule, are different for these compounds. The higher value of ΔE gap is found for **T2**, and it reflects its higher kinetic stability [45,46] expected due to symmetry reasons.

Taking into account our interest in complexing the HMs ions by these ligands, the donor–acceptor interactions were examined. They can occur between the π-electrons of the 2-thioxothiazolidin-4-one and the vacant d-orbital of the metal. As illustrated in **Figure 6.2**, HOMO orbitals are preferentially distributed on oxygen and Sulphur atoms of the rhodanine cycles. This is in good accordance with their ability to donate their vacant electrons and it is confirmed by the localization of the negative (red and orange regions) electrostatic potential (**Figure 6.3**). The complexation unit being the same, 2-thioxothiazolidin-4-one (rhodanine), the ligand's complexing capacity does not differ significantly, which is suggested by the small variance of the electrostatic potential (MinElPot). That observation leads to the assumption that a good complexation can be achieved for all the analyzed compounds.

From the graphical representation in **Figure 6.3** it is obvious that for all the investigated structures, the negative areas are mainly localized over the oxygen atoms (red regions). They correspond to the maximum negative values of potential (MinElPot—**Table 6.8**, line 16) which ranges as follows: −165.93 (**T1**) < −163.84 < (**T2**) −158.04 kJ.mol⁻¹ (**T3**). The maximum positive regions (blue) are localized on –NH group from rhodanine, assigned to atoms N1-H4, and vary in magnitude in the same order: 202.90 kJ/mol (for **T1**) < 203.27 (for **T2**) and 211.21 kJ.mol⁻¹ (for **T3**)

6.4.2.3. Correlation of molecular and QSAR properties

Attempts to find correlations between calculated molecular and QSAR properties (from **Table 6.8**) and the electron affinity (*A*) or ionization potential (*I*), respectively, are shown in **Table 6.11**. Linear relationships were considered for all parameters. The correlation coefficients of the linear dependencies (R^2) were of much help to establish correct connections. For instance, in terms of total energy for the correlation with *I* or *A*, R^2 is higher for *I* (0.995) than for *A* (0.613) when using the *ωB97XD* model. These values are higher than the corresponding ones obtained by the *B3LYP* method (0.846 and 0.684, respectively). For energy aq. R^2 is 0.613 for the correlation with *A* and 0.990 with *I* when using the *ωB97XD* model. For the *B3LYP* method, the values are lower, being 0.684 and 0.846 respectively. This protocol was followed for all the other properties from **Table 6.8**.

The best correlations for the parameters obtained by the two methods are collected in **Table 6.12** which gives the most confident dependencies and the method which led to such results. All the best correlations (R^2 over 0.9) were obtained with *I*, with one exception: the reduction potential which is correlated, as expected, with *A*. From the 13 best correlations, 11 were obtained using the *ωB97XD* model, which recommends the method as being more performant.

Table 6.11. "y = a + b•x" linear correlations between predicted molecular and QSAR properties and A or I, and their correlation coefficients (R^2) for **T1–T3** calculated using *B3LYP* /6-31G (d, p) and *ωB97XD*/6-311++G (d, p) density functional models, respectively, according to **Table 6.8**; *A* and *I* were expressed in eV. [66].

Correlated Parameters	a (intercept)		b (slop)		R^2	
	B3LYP	*ωB97XD*	*B3LYP*	*ωB97XD*	*B3LYP*	*ωB97XD*
Energy (y în au) *vs A* (x)	-3861.07	-2481.29	925.03	830.95	0.684	0.613
Energy (y în au) *vs I* (x)	-5985.35	-5470.54	604.83	730.42	0.846	0.995
Energy aq. (y în au) *vs A* (x)	-3861.02	-2481.38	925	830.95	0.684	0.613
Energy aq. (y în au) *vs I* (x)	-5985.13	-5470.376	604.80	730.39	0.846	0.990
Solvatation energy[*1] (y) *vs A* (x)	32.91	-20.41	-35.68	-31.94	0.598	0.521
Solvatation energy [*1] (y) *vs I* (x)	121.90	99.16	-24.29	-28.95	0.900	0.999
Dipole moment (y în D) *vs A* (x)	19.82	12.80	-4.73	-4.29	0.884	0.837
Dipole moment (y în D) *vs I* (x)	28.15	26.55	-2.75	-3.46	0.626	0.907
Oxidation potential (y în V) *vs I* (x)	-2.82	-3.46	0.61/	0.54	0.940	0.994
Ruduction potential (y în V) *vs A* (x)	-1.74	-1.62	0.08/	0.07	0.970	0.943
Area (y în $Å^2$) *vs A* (x)	1347.57	721.66	-416.79	-372.27	0.624	0.559
Area (y în $Å^2$) *vs I* (x)	2362.96	2093.01	-280.50	-333.26	0.886	0.999
Volume (y în $Å^3$) *vs A* (x)	1343.34	711.95	-420.50	-375.42	0.667	0.595
Volume (y în $Å^3$) *vs I* (x)	2326.24	2073.27	-277.30	-332.03	0.858	0.997
PSA (y în $Å^2$) *vs A* (x)	25.71	26.14	0.18	-0.11	0.50	0.235
PSA (y în $Å^2$) *vs I* (x)	25.22	nlc[*2]	0.13	nlc[*2]	0.945	nlc[*2]
Ovality index (y) *vs A* (x)	2.90	2.02	-0.59	-0.53	0.575	0.496
Ovality index (y) *vs I* (x)	4.01	4.40	-0.48	-0.40	0.999	0.913
Polarizability (y în 10^{-30} m^3) *vs A* (x)	97.73	149.68	-30.51	-34.12	0.587	0.662
Polarizability (y în 10^{-30} m^3) *vs I* (x)	229.81	208.77	-22.55	-27.06	0.862	0.998
LogP (y) *vs A* (x)	14.93	7.01	-5.27	-4.66	0.310	0.220
LogP (y) *vs I* (x)	31.49	26.73	-4.06	-4.65	0.992	0.944
MinElPOT (y în kJ·mol^{-1}) *vs A* (x)	-262.33	-200.84	40.26	31.17	0.869	0.611
MinElPOT (y în kJ·mol^{-1}) *vs I* (x)	-335.10	-313.08	23.63	27.42	0.651	0.995

[*1] (y in kJ·mol^{-1}); [*2] nlc = non-linear correlation.

Table 6.12. "y = a + b•x" corelații înclinate între proprietățile moleculare și QSAR prezise și *A* sau *I* pentru **T1-T3** calculate folosind modelele funcționale de densitate care ne-au oferit cei mai buni coeficienți de corelație (R^2); *A* și *I* am fost exprimați în eV [66].

Crt. Nr.	Correlated parameters	a (intercept)	b (slope)	R^2	DFT Method
1	Energy (y în au) *vs I* (x)	-5470.54	730.42	0.995	*ωB97XD*
2	Energy aq. (y în au) *vs I* (x)	-5470.38	730.39	0.990	*ωB97XD*
3	Solvatation energy[*1] (y) *vs I* (x)	99.16	-28.95	0.999	*ωB97XD*
4	Dipole moment (y în D) *vs I* (x)	26.55	-3.46	0.907	*ωB97XD*
5	Oxidation potential (y în V) *vs I* (x)	-3.46	0.54	0.994	*ωB97XD*
6	Reduction potential (y în V) *vs A*(x)	-1.74	0.08	0.970	*B3LYP*
7	Area (y în Å^2) *vs I* (x)	2093.01	-333.26	0.999	*ωB97XD*
8	Volume (y în Å^3) *vs I* (x)	2073.27	-332.03	0.997	*ωB97XD*
9	PSA (y în Å^2) *vs I* (x)	25.22	0.13	0.945	*B3LYP*
10	Ovality index (y) *vs I* (x)	4.01	-0.48	0.999	*B3LYP*
11	Polarizability (y în 10^{-30} m^3) *vs I* (x)	208.77	-27.06	0.998	*ωB97XD*
12	LogP (y) *vs I* (x)	31.49	-4.06	0.992	*B3LYP*
13	MinElPOT (y în kJ·mol^{-1}) *vs I* (x)	-313.08	27.42	0.995	*ωB97XD*

[*1] (y in kJ•mol^{-1})

6.4.2.4. Correlation of quantum chemical reactivity parameters

The main quantum parameters of the studied ligands calculated according to *B3LYP* /6- 31G (d, p) and *ωB97XD*/6-311++(d, p) models and given in **Table 6.9** show that *I* (line 1), χ (line 4) and ω (line 7) range in the order **T1** < **T2** < **T3**, regardless the chosen algorithm. This trend is in agreement with experiments that show the same order of complexation for the studied ligands. **T3** presents the highest values of these parameters, meaning that it has the highest total energy gain upon saturation with electrons, comparing to the other two ligands and explaining the experimental facts.

A (line 2), ΔE (line 3), η (line 5) and σ (line 6) do not show the same regular variation. The highest value for *A* is for **T3**; for **T1** and **T2**, the values for *A* are close. The highest values for ΔE and η are for **T2**, being close to those for **T3**. The highest value for σ is for **T1** being close to those of **T2** and **T3**. ΔE of **T3** is relatively smaller than **T2**. This fact indicates **T3** is more reactive than **T2**. Indeed, **T3** is found to be more able to interact in the complexation reaction of HMs (**Table 6.1**, lines 7–11). According to its lower ΔE, the most reactive compound among all seems to be **T1**. However, the experiments (**Table 6.1**, lines 7–11) show that **T1** has the lowest complexation ability. This discrepancy can be attributed to the lowest values for *A* and *I* for this ligand [66].

Table 6.13 shows the linear relationships considered for all quantum chemical reactivity parameters from **Table 6.9**, vs. *A* or *I*, respectively, as shown in the case of molecular and QSAR properties. The correlation coefficients of the linear dependencies (R^2) were used to establish correct connections. For instance, in terms of χ correlation with *I* or *A*, R^2 is higher for *I* (0.995) than for *A* (0.614) when using the $\omega B97XD$ model. For ω, a very good correlation was found with *A*, and the best correlation coefficient is obtained through the *B3LYP* model. η and σ are not linearly correlated with *A* and *I*. The best correlations for the parameters obtained by the two methods are collected in **Table 6.14** which gives the most confident dependencies and the method which led to such results.

Table 6.13. "y = a + b•x" linear correlations between predicted quantum chemical reactivity parameters and *A* or *I* (all expressed in eV) for **T1–T3** calculated using *B3LYP* /6-31G (d, p) and $\omega B97XD$/6-311++G (d, p) density functional models [66].

Crt. Nr.	Correlated parameters	a (intercept)		b (slope)		R^2	
		B3LYP	*ωB97XD*	*B3LYP*	*ωB97XD*	*B3LYP*	*ωB97XD*
1	χ (y) *vs A* (x)	1.21	3.04	1.09	1.06	0.806	0.614
2	χ (y) *vs I* (x)	-0.96	-0.76	0.66	0.93	0.734	0.995
3	η (y) *vs A* (x)	nlc[*]	nlc[*]	nlc[*]	nlc[*]	nlc[*]	nlc[*]
4	η (y) *vs I* (x)	0.38	1.83	0.14	0.24	0.458	nlc[*]
5	σ (y) *vs A* (x)	nlc[*]	nlc[*]	nlc[*]	nlc[*]	nlc[*]	nlc[*]
6	σ (y) *vs I* (x)	1.19	0.51	-0.07	-0.04	0.755	0.385
7	ω (y) *vs A* (x)	-1.29	1.34	2.67	1.37	0.999	0.956
8	ω (y) *vs I* (x)	-4.23	-2.63	1.31	1.03	0.227	0.754

[*] nlc = non-linear correlation

Table 6.14. "y = a + b•x" linear correlations between predicted quantum chemical reactivity parameters and *A* or *I* for **T1–T3** calculated using the density functional models which gave us the best correlations coefficients (R^2); all parameters are expressed in eV [66].

Crt. Nr.	Correlated parameter	a (intercept)	b (slope)	R^2	DFT Method
1	χ (y) *vs I* (x)	-0.76	0.93	0.995	*ωB97XD*
2	ω (y) *vs A* (x)	-1.29	2.67	0.999	*B3LYP*

The graphical quantities from **Figures 6.3–6.5** provide a visual representation of the chemically active sites, and allow the comparison of the local reactivity sites of the analyzed structures. The molecular electrostatic potential, previously discussed, is useful to identify the reactive sites for complexing interactions, and to understand the chemical recognition process based on this type of ligands.

The ionization potential map (**Figure 6.4**) is particularly useful to assess chemical reactivity and selectivity, in terms of electrophilic reactions. The blue color reveals the regions where ionization is relatively difficult. In these regions, localized over -NH group of Cycles III, the values of ionization potential vary as follows: 13.78 ÷ 14.83 (for **T1**), 13.84 ÷ 14.92 eV (for **T2**), and 13.84 ÷ 14.90 eV (for **T3**). The orange areas correspond to the lowest ionization potentials (most accessible to electrophiles), localized over Sulphur atoms from Cycles III. These sites present the following values: 7.06 ÷ 7.36 eV (for **T1**), 7.08 ÷7.44 eV (for **T2**) and 7.21 ÷ 7.47 eV (for **T3**) [66]. There are no red or orange areas on the local ionization potential maps, indicating there are no clear sites for electrophilic attack. This means the ligands were properly selected for complexation (which involves the nucleophilic attack of HMs ions).

The LUMO map (**Figure 6.5**) indicates nucleophilic reactivity. It can be observed that the colors are toward red, suggesting small values (near zero) of the LUMOs. Consequently, these ligands are not very susceptible to nucleophilic attack.

6.4.3. Correlations between DFT-calculated frontier molecular orbital's energies and experimental oxidation and reduction potentials

E_{HOMO} and E_{LUMO} predicted chemical parameters (**Table 6.8**) were correlated with experimental electrochemical properties resulted from the ligand characterization (**Table 6.1**) in order to establish the best ligand to be used for the complexation of HMs ions. Linear relationships obtained using *B3LYP* and *ωB97XD* hybrid functions for oxidation and reduction potentials (**Table 6.10**) are illustrated in **Figures 6.6**. R^2 values indicate satisfactory correlations between the calculated and the experimental values. The calculated HOMO orbital energies vary in the same order as the experimental values of the first anodic peak potentials, namely **T3** > **T2** > **T1**. The same behaviour was observed for the reduction capacity expressed as Ec1 experimental values, which varies in the opposite direction. So, the redox potential is influenced by the number and position of the alkyl groups, as assumed previously in [21,26,27]. Thus, the evaluation of the oxidation capacity of the investigated azulene systems is in good agreement with previously reported electrochemical data [47].

6.5. Conclusions on quantum mechanics calculations for (Z)-5-(azulen-1-yl methylene) -2-thioxothiazolidin-4-one derivatives

Quantum chemical calculations for three ligands derivatives of (Z)-5-(azulen-1-ylmethylene)-2-thioxothiazolidin-4-one are reported. They are structurally distinguished by the substitution of azulene cycle, respectively, by methyl and isopropyl groups: 3,8-Me$_2$- 5-iPr (**T1**), 4,6,8-Me$_3$ (**T2**) and H (**T3**). The chemical calculations resulted in a series of atomic (bond lengths, angles, Mulliken charges) and molecular descriptors particularly valuable in quantitative structure–activity relationships analysis and NMR spectra. These predicted chemical parameters were correlated with the experimental electrochemical characterization, in order to establish the best parameters for a ligand to be used for the complexation of HMs ions. Thus, the results of the evaluation of the oxidation capacity of the investigated azulene systems are in good agreement with previously reported electrochemical data. The calculated HOMO orbital energies vary in the same order as the experimental values of the first anodic peak potentials, namely **T3** > **T2** > **T1**. The same behaviour was observed for the reduction capacity which varies in the opposite direction, concluding that the redox potential is influenced by the number and position of the alkyl groups, in accordance with previous assumptions when designing the ligands. Linear correlations of DFT-calculated frontier molecular orbitals' energies and the experimental oxidation and reduction potentials were found. The computer-aided study turned out to be a complex structural approach, being an alternative to find parameters that matter when designing new ligands

Selective bibliographic references Chapter 6
[47] **A.-A. Vasile (Corbei),** E.-M. Ungureanu, G. Stanciu, M. Cristea, A. Ștefaniu, Evaluation of (Z)-5-(Azulen-1-ylmethylene)-2-thioxothiazolidin-4-ones properties using quantum mechanical calculations, Symmetry, 2021, 13, 1462.

Chapter 7. PROPERTIES ASSESSEMENT BY QUANTUM MECHANICAL CALCULATIONS FOR AZULENES SUBSTITUTED WITH THIOPHENE-VINYL-PYRIDINE OR FURAN-VINYL-PYRIDINE

7.1. Properties of azulenes substituted with thiophenes-vinyl-pyridine or furan-vinyl-pyridine

Chemically modified electrodes (CMEs) obtained by electrochemical polymerization of differently substituted azulene monomers have been tested and characterized by electrochemistry [1, 2] in the *Laboratory of Electrochemical Processes in Organic Solvents (PESO).* The above data refer to heavy metal ion (HMs) recognition tests to detect very low concentrations of contaminants such as cadmium, copper, mercury, chromium, cobalt, nickel or lead in water [3-5] . The advantage is certain in the context of health concerns due to the harmful effects of these HMs on humans; their bioaccumulation in the human body causes acute or chronic toxicity, responsible for serious disorders especially in long-term exposure. New research has emerged linking the onset of progressive degenerative physical and neurological lesions, such as Parkinson's and Alzheimer's disease or even cancer, and the accumulation of HMs. [6-9]. Although essential heavy metals are key components of several enzymes involved in biochemical processes and perform important physiological functions, for example, copper as a co-factor of enzymes related to oxidative stress [10] or constituent of metal enzymes responsible for hemoglobin formation [11]), the danger of them becoming toxic contaminants must be controlled and prevented.

As part of the *PESO* Laboratory's ongoing interest in developing methodologies for the multifunctionality of azulenes [12], the electrochemistry of a series of 4- (azulen-1-yl) pyridine was investigated (**Figure 7.1**). The investigated compounds are furan–vinyl–pyridine–azulenes (**O1**–**O3**) and thiophen–vinyl–pyridine–azulenes (**S1–S3**). The grafted pyridines were attached in position 1 to 5-isopropyl-3,8-dimethylazulene (**O1** and **S1**), 4,6,8-trimethylazulene (**O2** and **S2**), or azulene (**O3** and **S3**), respectively.

This compounds interact with metal ions due to the property of 2,6-bis((E)-2-(furan/thiophene-2-yl)vinyl)pyridine, which is a Lewis base. They are all valuable synthons for the synthesis of highly conjugated aromatic systems [13,14]. In connection to their capacity to polymerize, they are useful for constructing novel analytical materials for sensor applications [15-17].
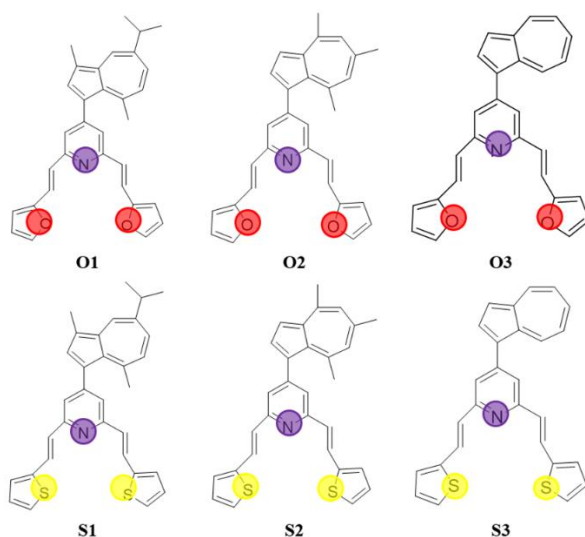
Figure 7.1. Structure of the studied molecules.

The structures of the ligands for which quantum mechanics calculations were performed [18] presented in this chapter of the thesis are presented in **Figure 7.1.**

The compounds calculated in this chapter of the thesis contain a part of pyridine known for its HMs complexing properties [19]. 4-(azulen-1-yl) pyridines substituted with furyl-vinyl or thienyl-vinyl lead to more extensive conjugate systems that are easy to polymerize. The electrochemistry of a series of new 4- (azulen-1-yl) pyridines that were synthesized at the *Center for Organic Chemistry of the Romanian Academy* was investigated [20]. Some of the synthesized compounds were integrated into the graphite paste resulting in **S2** isomer modified electrodes, which exhibited Zn sensor properties

[21]. The study of the **O1** ligand by electrochemical methods led to the finding of the best potential at which this azulene can be polymerized. The literature shows that the electrodes modified with the molecules in **Figure 7.1** were used for the recognition of HMs by preconcentration and anodic stripping. The best result was observed for Pb (detection limit of 10^{-7} M) [4]. The electrochemical study of the **S1** ligand led to the establishment of the best conditions for obtaining CMEs that were tested for the recognition of HMs cations, with the best results for lead and copper at concentrations lower than 10^{-8} M [3]. Recognition of HMs ions has recently been reported for modified electrodes based on **O3** and **S3** ligands [22, 23]. Using these experimental data in this thesis, calculations of chemical parameters were performed to estimate / predict which of the parameters of these ligands can be correlated with the experimental electrochemical properties resulting from the characterization of the ligands. The calculations are consistent with literature data for other ligands that can be used to complex HM ions (with low detection limits) [24].

In silico studies of thiophenyl-vinyl-pyridine or furan-vinyl-pyridine-substituted azulenes were performed using Functional Density Theory (DFT) in order to obtain structural details for ligands [25, 26]. Recent similar data on other azulene structures have revealed linear correlations of the energies of frontier molecular orbitals calculated by DFT and experimental oxidation and reduction potentials [27]. Thus, the computer-assisted investigation proved a relevant approach to identify the key parameters for the design of new ligands with better electrochemical properties. In general, the previous calculations are based on the correlation of the electrochemical oxidation and reduction potential, with the energy levels corresponding to the highest occupied molecular orbital (HOMO) or, respectively, the lowest unoccupied molecular orbital (LUMO), [28-30]. For such quantum calculations, the use of the *B3LYP* functional density model has led to strong linear correlations between HOMO / LUMO orbital energy and redox potentials [31]. More accurate results were obtained using the *ωB97XD* functional [27, 32]. DFT calculations provided precise structural details and predictive properties that were well correlated with the electrochemical behavior and other properties of the investigated ligands.

7.3. Results of calculations of the properties of azulene substituted with furan-vinyl-pyridine (O1-O3) and thiophene-vinyl-pyridine (S1-S3)

7.3.1. Molecular and QSAR properties computations

Table 7.3 shows the predicted molecular properties ([a-g]) and QSAR ([h-m]) resulting from DFT calculations using *B3LYP* and *ωB97XD* density functional models for the investigated ligands. In addition to the total energy E (in atomic units, au), estimates are also given for the energy of the solvated molecule (E_{aq}) and the difference between Eaq and E which represents the solvation energy (E_{solv}, in kJ / mol^{-1}) [44].

Starting from the electronic properties, materialized in the energies E_{HOMO} and E_{LUMO} and presented in **Table 7.3**, other related quantum descriptors were calculated. According to Koopman's theorem [45, 46], E_{HOMO} is related to the ionization potential ($I = - E_{HOMO}$), and E_{LUMO} to the affinity of electrons ($A = - E_{LUMO}$). The difference between the energies of the molecular orbitals HOMO and LUMO ($\Delta Egap$), the absolute electronegativity ($\chi = (I + A) / 2$), the global hardness ($\eta = (I - A) / 2$), the property of being soft were also calculated, which is the inverse of hardness, softness ($\sigma = 1 / \eta$) [47, 48], and values of the global electrophilicity index ($\omega = m^2 / 2\eta$) [49]. **Table 7.4** gives the calculated values, using the DFT models *B3LYP* and *ωB97XD*, for the quantum parameters of chemical reactivity for all 6 compounds investigated [18].

Table 7.3. Predicted molecular [a–g] and QSAR [h–m] properties of oxygen (**O1**, **O2**, **O3**) and sulfur (**S1**, **S2**, **S3**) compounds calculated using *B3LYP* and *ωB97XD* DFT models.

Parameter	O1 $C_{32}H_{29}NO_2$		O2 $C_{30}H_{25}NO_2$		O3 $C_{27}H_{19}NO_2$	
	B3LYP	*ωB97XD*	*B3LYP*	*ωB97XD*	*B3LYP*	*ωB97XD*
M [a] (g·mol^{-1})	459.59		431.54		389.45	
E [b] (au)	-1441.98	-1441.51	-1363.36	-1362.9	-1245.42	-1244.99
E_{aq} [c] (au)	-1441.99	-1441.52	-1363.37	-1362.91	-1245.43	-1245
E_{solv} [d] (kJ·mol^{-1})	-23.72	-21.35	-27.97	-25.92	-32.7	-30.16
μ [e] (D)	3.10	3.27	3.43	3.67	2.91	3.11
E_{HOMO} [f] (eV)	-4.92	-6.74	-5.08	-6.93	-5.12	-7.03
E_{LUMO} [g] (eV)	-1.79	-0.13	-1.77	-0.13	-2.04	-0.36
S [h] (Å^2)	520.42	514.08	481.21	474.27	429.84	423.09
V [i] (Å^3)	508.94	506.68	472.01	469.83	418.75	416.98
PSA [j] (Å^2)	18.27	16.79	18.31	16.80	18.6	17.93
OI [k]	1.69	1.67	1.64	1.62	1.59	1.57
a [l] (10^{-30}·m^3)	81.92	80.91	78.88	77.88	74.61	73.62
E_{pot} [m] (kJ·mol^{-1})	-166.66	-167.73	-167.67	-168.84	-164.84	-163.65
Parameter	S1 $C_{32}H_{29}NS_2$		S2 $C_{30}H_{25}NS_2$		S3 $C_{27}H_{19}NS_2$	
	B3LYP	*ωB97XD*	*B3LYP*	*ωB97XD*	*B3LYP*	*ωB97XD*
M [a] (g·mol^{-1})	491.72		463.67		421.59	
E [b] (au)	-2087.94	-2087.47	-2009.31	-2008.86	-1891.37	-1890.95
E_{aq} [c] (au)	-2087.95	-2087.48	-2009.32	-2008.88	-1891.38	-1890.96
E_{solv} [d] (kJ·mol^{-1})	-32.25	-32.25	-36.99	-37.13	-39.55	-38.56
μ [e] (D)	3.11	3.22	3.33	3.55	2.79	2.82
E_{HOMO} [f] (eV)	-4.98	-6.72	-5.13	-6.91	-5.27	-7.07
E_{LUMO} [g] (eV)	-1.84	-0.14	-1.83	-0.14	-2.06	-0.36
S [h] (Å^2)	535.76	532.51	496.12	491.29	444.51	442.36
V [i] (Å^3)	526.71	524.23	489.67	487.32	436.52	434.71
PSA [j] (Å^2)	6.297	6.187	6.34	6.21	6.31	6.25
OI [k]	1.70	1.69	1.65	1.64	1.60	1.59
a [l] (10^{-30}·m^3)	83.36	82.34	80.32	79.31	76.03	75.05
E_{pot} [m] (kJ·mol^{-1})	-160.04	-152.77	-165.18	-154.99	-159.77	-160.26

[a] molecular weight (M); [b] total energy (E); [c] aqueous solvation energy (E_{aq}); [d] solvation energy (E_{solv}), [e] dipole moment (μ); [f] energy of the HOMO orbital (E_{HOMO}); [g] energy of the LUMO orbital (E_{LUMO}); [h] area (S), [i] volume (V); [j] polar surface area (PSA); [k] ovality index (OI) (degree of deviation from perfect spherical shape molecule); [l] polarizability (a); [m] minimum value of electrostatic potential (E_{pot}).

The variation of the minimum values of the electrostatic potential, E_{pot} (**Table 7.3**) for each compound can be viewed in the electrostatic potential (EPM) maps. They allow the evaluation of reactive sites in a molecule [50]. The EPMs for the investigated **O1-O3** and **S1-S3** compounds are shown in **Figure 7.13** and **Figure 7.14**, respectively, which show red and blue areas for the negative and positive regions susceptible to electrophilic and nucleophilic attacks, respectively.

The frontier molecular orbitals density distribution calculated by using *B3LYP* , which resulted from the quantum calculation for oxygen compounds (**O1-O3**) are shown in **Figure 7.15**, along with the energy levels and their gaps (*ΔEgap*) between HOMO and LUMO (**Table 7.4**). Similarly, the representation of FMOs density distribution [51] for **S1-S3** sulfur compounds is given in **Figure 7.16**.

The positive and negative regions phases of the frontier molecular orbitals are represented by red and blue, respectively.

Table 7.4. Quantum chemical reactivity parameters of investigated compounds calculated using *B3LYP* and *ωB97XD* DFT models [18].

Parameter	O1 $C_{32}H_{29}NO_2$		O2 $C_{30}H_{25}NO_2$		O3 $C_{27}H_{19}NO_2$	
	B3LYP	*ωB97XD*	*B3LYP*	*ωB97XD*	*B3LYP*	*ωB97XD*
$I^m = -E_{HOMO}$ (eV)	4.92	6.74	5.08	6.93	5.12	7.03
$A^n = -E_{LUMO}$ (eV)	1.79	0.13	1.77	0.13	2.04	0.36
$\Delta E_{gap}{}^o = I - A$ (eV)	3.13	6.61	3.31	6.8	3.08	6.67
$\chi^p = (I+A)/2$ (eV)	3.36	3.44	3.43	3.53	3.58	3.70
$\eta^q = (I-A)/2$ (eV)	1.57	3.31	1.66	3.40	1.54	3.34
$\sigma^r = 1/h$ (eV^{-1})	0.64	0.30	0.60	0.29	0.65	0.30
$\omega^s = m^2/2h$ (D· eV^{-1})	3.07	1.62	3.55	1.98	2.75	1.45
	S1 $C_{32}H_{29}NS_2$		S2 $C_{30}H_{25}NS_2$		S3 $C_{27}H_{19}NS_2$	
	B3LYP	*ωB97XD*	*B3LYP*	*ωB97XD*	*B3LYP*	*ωB97XD*
$I^m = -E_{HOMO}$ (eV)	4.98	6.72	5.13	6.91	5.27	7.07
$A^n = -E_{LUMO}$ (eV)	1.84	0.14	1.83	0.14	2.06	0.36
$\Delta E_{gap}{}^o = I - A$ (eV)	3.14	6.58	3.30	6.77	3.21	6.71
$\chi^p = (I+A)/2$ (eV)	3.41	3.43	3.48	3.53	3.67	3.72
$\eta^q = (I-A)/2$ (eV)	1.57	3.29	1.65	3.39	1.61	3.36
$\sigma^r = 1/h$ (eV^{-1})	0.64	0.30	0.61	0.30	0.62	0.30
$\omega^s = m^2/2h$ (D· eV^{-1})	3.08	1.58	3.36	1.86	2.42	1.19

[m] ionization potential (*I*); [n] electron affinity (*A*); [o] energy gap (ΔE_{gap}); [p] electronegativity (*χ*); [q] global hardness (*η*); [r] softness (σ); [s] global electrophilicity index (*ω*).
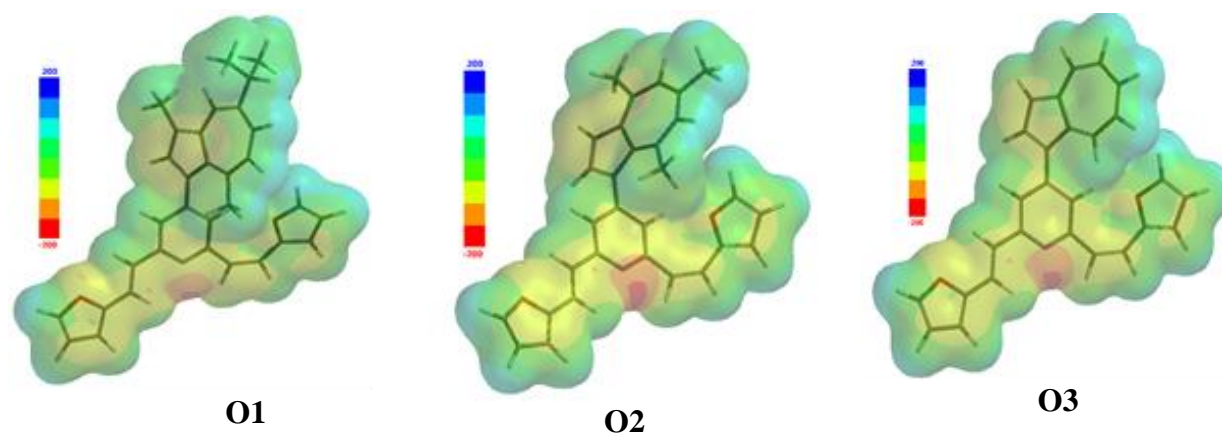

Figure 7.13. Electrostatic potential map (EPM) for compouns **O1**–**O3,** calculated with *Spartan 14 Software.*

7.3.2. Correlations between DFT-calculated frontier molecular orbital's energies and experimenta data

The calculated HOMO and LUMO energies were correlated with the experimental oxidation and reduction potentials of the investigated compounds. Electrochemical experiments to obtain these values were performed by Differential Pulse Voltammetry (DPV). This method is considered to be one of the most accurate methods for assessing the potential of a particular process. The experimental oxidation / reduction potential was evaluated as the potential of the first anodic / cathodic DPV peak, denoted *Ea* and *Ec*, respectively. The values *Ea* (V) and Ec (V) are listed in **Table 7.5** for compounds **O1-O3** and, respectively, **S1-S3**. Data were collected in 0.5 mM solutions of each ligand, in 0.1 M tetrabutylammonium perchlorate in acetonitrile [3-5, 22, 23].

Table 7.5. Experimental oxidation (*Ea*) and reduction (*Ec*) potentials [3-5, 17, 19] for **O1 – O3** and **S1 – S3** ligands.

Property	Ligand		
	O1	**O2**	**O3**
E_a (V)	0.318	0.487	0.553
E_c (V)	-2.071	-2.084	-1.854
Reference	[4]	[2]	[23]
	S1	**S2**	**S3**
E_a (V)	0.338	0.470	0.567
E_c (V)	-2.065	-2.090	-1.858
Reference	[3]	[5]	[22]

The calculated HOMO and LUMO energies (**Table 7.3**.) Were plotted against the experimental oxidation and reduction potentials and linear relationships were observed. The reduction and oxidation potentials were correlated with both the ionization potential (*I*) and the electron affinity (*A*) calculated using the *B3LYP* and *ωB97XD* hybrid functionalities (**Table 7.4**). The parameters of the obtained linear correlations (a-intercept, b-slope and R^2-correlation coefficient) are presented in **Table 7.6.**

Table 7.6. Values of intercept (a), slope (b), and correlation coefficient (R^2) from the linear correlation obtained for the oxidation (*Ea*) and reduction (*Ec*) potentials with *I* and *A*, respectively, for the investigated ligands from computations with *B3LYP* or *ωB97XD* hybrid functionals.

Correlation	*B3LYP*			*ωB97XD*		
	a	*b*	*R^2*	*a*	*b*	*R^2*
O1-O3						
Ea vs. I	-5.298	1.141	0.993	-5.211	0.821	0.995
Ec vs. A	-3.606	0.859	0.9997	-2.204	0.972	0.998
S1-S3						
Ea vs. I	4.500	1.259	0.995	6.202	1.523	0.999
Ec vs. A	3.949	1.017	0.996	2.199	0.991	0.990

7.3.3. Correlations between DFT-calculated and QSAR properties and ionization potential (*I*) or electron affinity (*A*)

Correlations between calculated molecular properties (*E, E_{aq}, E_{solv}, μ*) and QSAR (*S, V, PSA, OI, α, E_{pot}*) (from **Table 7.3**) and ionization potential (*I*) or electron affinity (*A*) are shown in

Tablessele 7.7 and **7.8**. Linear relationships (*a* - intercept, *b* - slope, and R^2 - correlation coefficient) were considered for most parameters. [18].

Table 7.7. Linear correlations between predicted molecular properties and ionization potential (*I*) or electron affinity (*A*), computed using *B3LYP* and *ωB97XD* hybrid functionals; *A* and *I* are expressed in eV

Correlation	B3LYP			ωB97XD		
	a	*b*	R^2	*a*	*b*	R^2
O1-O3						
E vs. I	-5595.9	842.39	0.812	-5786.5	642.99	0.917
E vs. A	-2441.8	584.77	0.791	-1491.1	683.54	0.842
Eaq vs. I	-5595.9	842.39	0.812	-5786.5	642.99	0.917
Eaq vs. A	-2441.8	584.77	0.791	-2441.8	584.77	0.791
Esolv vs. I	171.76	-39.66	0.870	178.07	-29.55	0.980
Esolv vs. A	19.12	-25.31	0.720	-19.95	-28.37	0.730
μ vs. I	nlc**			nlc**		
μ vs. A	nlc**			nlc**		
S1-S3						
E vs. I	-5461.8	676.00	0.982	-5838.5	556.91	0.973
E vs. A	-3306.9	686.25	0.813	-2148.2	714.61	0.842
Eaq vs. I	-5461.9	676.00	0.982	-5838.5	556.91	0.973
Eaq vs. A	-3306.9	686.25	0.813	-2148.2	714.64	0.842
Esolv vs. I	93.18	-25.25	0.977	90.05	-18.27	0.936
Esolv vs. A	nlc**			nlc**		
μ vs. I	nlc**			nlc**		
μ vs. A	6.784	-1.941	0.863	3.745	-2.568	0.796

* The significance of the properties is the same as in **Tables 7.3** and **7.4**; ** nlc – non-linear correlation.

Table 7.8. Linear correlations between predicted QSAR properties and ionization potential (*I*) or electron affinity (*A*), computed using *B3LYP* and *ωB97XD*; *A* and *I* are expressed in eV.

Correlation	B3LYP			ωB97XD		
	a	*b*	R^2	*a*	*b*	R^2
O1-O3						
S vs. I	2460.50	-393.52	0.841	2541.00	-300.07	0.939
S vs. A	968.30	-263.11	0.760	534.35	-309.07	0.809
V vs. I	2422.40	-388.05	0.802	2494.20	-294.16	0.924
V vs. A	964.01	-266.49	0.782	528.54	-309.89	0.833
PSA vs. I			nlc**			nlc**
PSA vs. A	16.19	1.18	0.969	16.15	4.94	0.999
OI vs. I	3.89	-0.45	0.893	3.93	-0.33	0.969
OI vs. A	2.16	-0.28	0.690	1.69	-0.33	0.750
α vs. I	237.41	-31.54	0.826	242.59	-23.93	0.927
α vs. A	118.60	-21.50	0.776	82.66	-25.11	0.829
Epot vs. I			nlc**			nlc**
Epot vs. A	-183.43	9.13	0.916	-170.90	20.15	0.959

Table 7.8

Correlation	B3LYP			ωB97XD		
	a	*b*	*R²*	*a*	*b*	*R²*
S1-S3						
S vs. I	2102.20	-314.06	0.991	2257.30	-256.31	0.990
S vs. A	1086.40	-311.13	0.781	556.15	-316.09	0.791
V vs. I	2074.80	-310.24	0.985	2233.80	-253.87	0.978
V vs. A	1081.30	-312.58	0.804	551.00	-323.02	0.832
PSA vs. I		nlc**		4.99	0.1782	0.959
PSA vs. A		nlc**		6.17	0.2341	0.870
OI vs. I	3.42	-0.345	0.999	3.61	-0.285	0.998
OI vs. A	2.28	-0.3254	0.716	1.71	-0.3409	0.750
α vs. I	209.18	-25.216	0.987	221.57	-20.678	0.979
α vs. A	128.29	-25.334	0.799	84.50	-26.25	0.829
E_{pot} *vs. I*		nlc**		-10.42	-21.099	0.923
E_{pot} *vs. A*		nlc**		-149.82	-29.00	0.917

* The significance of the properties is the same as in **Tables 7.3** and **7.4**; ** nlc – non-linear correlation

7.3.4. Correlation of quantum chemical reactivity parameters

The quantum chemical reactivity parameters for the investigated compounds, obtained with the *B3LYP* and *ωB97XD* functionalities, were also correlated with the ionization potential (*I*) and the electronic affinity (*A*). Linear correlations have been proposed for each quantum parameter of chemical reactivity. The obtained correlation parameters (*a, b* and R^2) were presented in **Table 7.9** for each type of correlation.

Table 7.9. Linear correlations between the predicted quantum chemical reactivity parameters and the ionization potential (*I*) and the electronic affinity (*A*), respectively; *A* and *I* are expressed in eV.

Correlation	B3LYP			ωB97XD		
	a	*b*	*R²*	*a*	*b*	*R²*
O1-O3						
χ vs. I		nlc**			nlc**	
χ vs. A	2.0664	0.743	0.942	3.3624	0.9239	0.870
η vs. I	4.4667	-0.5714	1.000	5.1432	-0.2604	0.624
η vs. A		nlc**			nlc**	
σ vs. I	0.4941	0.2232	0.999	0.14	0.023	0.617
σ vs. A		nlc**			nlc**	
ω vs. I	21.971	-3.7393	0.954	14.382	-1.8404	0.999
ω vs. A		nlc**			nlc**	
S1-S3						
χ vs. I		nlc**			nlc**	
χ vs. A	1.6338	0.9867	0.948	3.3264	1.0795	0.893
η vs. I		nlc**			nlc**	
η vs. A		nlc**			nlc**	
σ vs. I		nlc**			nlc**	
σ vs. A		nlc**			nlc**	
ω vs. I	19.407	-3.2091	0.940	14.783	-1.9129	0.981
ω vs. A	9.6175	-3.4881	0.892	2.0581	-2.4249	0.823

* The significance of the properties is the same as in **Table 7.4**; ** nlc – non-linear correlation.

7.4. Discussions on the study of the properties of furans substituted with furan-vinyl-pyridine (O1-O3) and thiophene-vinyl-pyridine (S1-S3)

The values calculated from **Table 7.3** using the *B3LYP* and *ωB97XD* functionalities are quite similar for *E, Eaq, OI, α, Epot*. The values calculated with the *B3LYP* hybrid functional are generally slightly higher (in absolute value), with exceptions for the dipole moment (μ) and E$_{HOMO}$. Also, the *Esolv* values for **S1** and **S2** are equal to or less when using the *B3LYP* function than *ωB97XD*.

The dipole moment for oxygen and sulfur compounds varies in the order: **O2> O1> O3** and **S2> S1> S3**, respectively, which is the same as for the absolute values of the minimum value of the electrostatic potential: **O2> O1> O3** and **S2> S1 > S3**. Both properties and amounts are used to describe the polarity of the molecule and indicate that the unsubstituted compound is the least polar and the substituted ones are more polar. Replacement of hydrogen atoms in azulene with the methyl group or the isopropyl group results in a systematic increase in the minimum value of the electrostatic potential for both types of compounds, which can be explained by the inductive + *I* effects of the alkyl groups.

The values calculated for the quantum parameters of chemical reactivity in **Table 7.4**, predicted with the functionalities *B3LYP* and *ωB97XD* are quite different. For parameters *I, ΔEgap, χ, η*, the values calculated with the functional *ωB97XD* are significantly higher than the values calculated with **B3LYP**. For parameters *A, σ* and *ω* the situation is inverse (**Table 7.4**). These results are valid for all compounds investigated.

In terms of *ΔEgap* values, **O3** shows the lowest *ΔEgap* and **O2** the highest. This can be explained by the substitution of the azulene ring with methyl or isopropyl groups (with inductive effects + *I*) which results in a systematic increase in LUMO energy and an increase in the absolute value for the reduction potential.

Regardless of the function used for the calculation, it can be seen that the ionization potential (*I*) varies in the order **O1 <O2 <O3**. This behavior is also observed for sulfur compounds. Electronic affinity values (*A*) do not show the same regular variation. The highest value of *A* is for **O3**; for **O1** and **O2** the values of *A* are relatively close. For sulfur compounds, **S3** also has the highest value for electron affinity, for **S1** and **S2** the values of *A* are relatively close (**Table 7.3**).

Since the interest pursued in the study of these ligands is the complexation of heavy metal ions, the donor-acceptor interactions were examined by following several parameters: *ΔEgap*, global electrophilicity index, etc. The descriptor that was used to represent molecular stability is the difference between the HOMO and LUMO (*ΔEgap*) energy levels that quantify the possible charge transfer interactions within the molecule. The higher the apEgap, the more stable the compound. The higher value of *ΔEgap* for **O2** and **S2** in their homologous series leads to the conclusion that the substituted structures are more stable (**Table 7.4**). Thus, the most reactive compounds appear to be the unsubstituted ones (**O3** and **S3**), which are most intensely involved in the HMs complexation process.

A molecule with a small *ΔEgap* is generally associated with high chemical reactivity, low kinetic stability, and high polarizability [52]. The unsubstituted compound **O3**, which has the smallest energy gap (**Table 7.4**), has the lowest polarizability (α), which means that it is the most reactive (**Table 7.3**).

The higher value of the global electrophilicity index for symmetrically substituted azulene compounds (**O2** and **S2**) suggests that they are more electrophilic than the unsubstituted compounds (**O3** and **S3**).

The graphical representations illustrated in **Figures 7.13** and **7.14** indicate the chemically active regions and facilitate the comparison of the local reactivity zones of the investigated structures. The red zone (negative charge) is found around the electronegative N in pyridine, which suggests reactive sites for the complexation of these ligands on HMs ions. The red region is susceptible to electrophilic attack. These negative areas correspond to the most negative potential values (*Epot* values in **Table 7.3**). The values of the Epot potential for oxygen compounds are ordered as follows: **O2> O1> O3**, regardless of the function used in the calculation. For the sulfur series, the order is similar for the

B3LYP functional (**Table 7.2**), ie: **S2> S1> S3**, but is slightly different for the *ωB97XD* functional (**S3> S2> S1**).

Comparatively, as expected, oxygen compounds have lower electrostatic potentials in absolute terms than sulfur compounds, as shown by the variation in red intensity (**Figures 7.13** and **7.14**).

Recently published molecules (relating to (Z)-5-(azulen-1-ylmethylene) -2-thioxothiazolidin-4-one) [27] which have in common with the ligands analyzed in this chapter azulene rings, including the same substituents on azulene, they have a smaller frontier gap orbit. This shows that they are more reactive than the investigated compounds **O1-O3** and **S1-S3**. Thioxothiazolidin-4-one molecules also have a higher value of the overall electrophilicity index (values around 5 D / (eV) [27] compared to the molecules investigated (**Table 7.4**) in this study (values in about 3 D / (eV)), suggesting that the ligands in [27] are more electrophilic than **O1-O3** and **S1-S3**.

The distribution of HOMO orbitals for oxygen compounds (**Figure 7.15**) is located on azulene and pyridine rings for **O1** and **O2** compounds. For **O3**, they are located on the furan-vinyl-pyridine-vinyl-furan conjugate system. For sulfur compounds (**Figure 7.16**), HOMO orbitals are distributed on the azulene and pyridine rings for compounds **S1** and **S2** and on the whole molecule in the case of **S3**. The difference between the distribution of HOMO orbitals in the case of **O1**, **O2** and **O3** is a very important result obtained from the calculations performed, because they are related to the oxidation capacity of these ligands, which is a key parameter in the electropolymerization of these structures.

For both oxygen and sulfur compounds, the LUMO distribution is located on the azulene rings (**Figures 7.15** and **7.16**).

Given the interest of this study related to the recognition of HMs ions by complexation with these ligands, donor-acceptor interactions were examined. They can occur between the pair of non-participating electrons of the N and the vacant *d* orbital of the heavy metal.

The electrochemical oxidation and reduction potentials were read from the DPV curves, which more precisely indicate the first processes that take place during anodic or cathodic scans. The electrochemical oxidation potentials (*Ea)* for both oxygen and sulfur compounds (**Table 7.5**) vary in the order of **O3 > O2 > O1** and **S3 > S2 > S1**, respectively, indicating higher values for *Ea* in the case of compounds unsubstituted compounds which decrease in the case of compounds with different substituents with + *I* inductive effects. The electrochemical reduction potentials *Ec* (in absolute value) for both oxygen and sulfur compounds (**Table 7.5**) vary in reverse order: **O2 > O1 > O3** and **S2 > S1 > S3**, respectively. Substitution of hydrogen atoms in azulene with methyl (-CH$_3$) or isopropyl groups results in an increase in the absolute value of the reduction potential with respect to the unsubstituted compound, but the usual behavior is complicated by symmetry because **O2** is more symmetric than **O1**, and its reduction is more difficult.

The predicted quantum parameters E$_{HOMO}$ and E$_{LUMO}$ (**Table 7.3**) were correlated with the experimental electrochemical properties resulting from the characterization of the ligand (**Table 7.5**). Linear relationships were obtained using both the *B3LYP* and *ωB97XD* hybrid functionalities. (Table 7.6). R^2 values indicate very good correlations between calculated and experimental values for both functional (greater than 0.990).

The energies of the calculated HOMO orbitals vary in the same order for the oxygen and sulfur compounds as the experimental values of the potentials for the first anodic peaks, namely **O3> O2> O1** and **S3> S2> S1** (absolute values). Thus, the evaluation of the oxidation capacity of the investigated azulenes is in good agreement with the electrochemical data.

The same order of variation for both *Ea* and Ec is observed for six similar compounds, derived from 4- (azulen-1-yl) -2,6-bis (2-furyl) - and 4- (azulen-1- il)-2,6-bis (2-thienyl) -pyridines, which have been previously investigated [53].

Table 7.7 and **Table 7.8** show correlations between the calculated molecular properties (**Table 7.3**) and the QSAR properties (**Table 7.4**) and the ionization potential (*I*) or, respectively, the electronic affinity (*A*). Linear relationships for all parameters were taken into account. The correct connections

were chosen using the dependencies that have the highest linear correlation coefficients (R^2). For example, the value of R^2 for the correlation of total energy (E) with I (0.917 in **Table 7.7**) is higher than for the correlation corresponding to A (0.842) when using the functional ωB97XD. Moreover, these values are higher than those obtained using the *B3LYP* functional (0.812 and 0.791 respectively) [18].

The value of R^2 for the correlation of the solvation energy of the molecule (*Eaq* in **Table 7.7**) with *A* (0.791) is lower than that for the correlation with *I* (0.917), when the functional ωB97XD is used. When using the *B3LYP* function, both values are lower, 0.719 and 0.783, respectively. This protocol was followed for all other properties indicated in **Table 7.3**.

Table 7.10 shows the best correlations of the parameters (R^2 over 0.9) and the functional that led to their obtaining. For oxygen compounds, the best correlations were obtained using the functional ωB97XD hybrid. Dependencies on ionization potential *I* are linear, except for PSA and *Epot*, which are better correlated with *A*. For sulfur compounds the best correlations were obtained with *I*, most using the *B3LYP* functional [18].

Table 7.9 shows the linear correlations for the quantum parameters of chemical reactivity in *Table 7.4*, with *A* and *I*, respectively. For oxygen compounds, the correlations of η, σ and ω are better with *I* than with *A*, while the correlation χ (*A*) is better than χ (*I*). The best correlation coefficient is obtained by the *B3LYP* hybrid functional. For sulfur compounds, the correlations are weaker than for oxygen compounds. Therefore, good correlations were found only for χ (*A*) and ω (*I*), when using the *B3LYP* functional hybrid. The ωB97XD hybrid functional has a good correlation only for ω (*I*) for both oxygen and sulfur compounds. **Table 7.11** shows the best correlations of the parameters (R^2 over 0.9) and the functional used to obtain them [18].

Table 7.10. Linear correlations "y = a + b.x" between the predicted molecular properties and QSAR* and *I* or A for the investigated compounds, calculated using the functional density models that led to the best correlation coefficients (R^2); *A* and *I* are expressed in eV.

Correlated parameter	*a*	*b*	R^2	**DFT Method**
O1 - O3				
E vs. *I*	-5786.5	642.99	0.917	*ωB97XD*
Eaq vs. *I*	-5786.5	642.99	0.917	*ωB97XD*
Esolv vs. *I*	178.07	-29.55	0.980	*ωB97XD*
S vs. *I*	2541.00	-300.07	0.939	*ωB97XD*
V vs. *I*	2494.20	-294.16	0.924	*ωB97XD*
PSA vs. *A*	16.15	4.94	0.999	*ωB97XD*
OI vs. *I*	3.93	-0.33	0.969	*ωB97XD*
α vs. *I*	242.59	-23.93	0.927	*ωB97XD*
Epot vs. *A*	-170.90	20.15	0.959	*ωB97XD*
S1 – S3				
E vs. *I*	-5461.8	676.00	0.982	*B3LYP*
Eaq vs. *I*	-5461.9	676.00	0.982	*B3LYP*
Esolv vs. *I*	93.18	-25.25	0.977	*B3LYP*
S vs. *I*	2102.20	-314.06	0.991	*B3LYP*
V vs. *I*	2233.80	-253.87	0.978	*ωB97XD*
PSA vs. *I*	4.99	0.1782	0.959	*ωB97XD*
OI vs. *I*	3.42	-0.345	0.999	*B3LYP*
α vs. *I*	209.18	-25.216	0.987	*B3LYP*
Epot vs. *I*	-10.42	-21.099	0.923	*ωB97XD*

* The significance of the properties is the same as in **Table 8.1**

Table 7.11. Linear correlations "y = a + b.x" between the quantum parameters of predicted chemical reactivity * and *A* or *I* for the investigated compounds, calculated using the functional density models that led to the best correlation coefficients (R^2); A and *I* are expressed in eV.

Correlated parameter	*a*	*b*	*R^2*	DFT Method
O1 - O3				
χ *vs. A*	2.0664	0.743	0.942	*B3LYP*
η *vs. I*	4.4667	-0.5714	1.000	*B3LYP*
σ *vs. I*	0.4941	0.2232	0.999	*B3LYP*
ω *vs. I*	21.971	-3.7393	0.954	*B3LYP*
ω *vs. I*	14.382	-1.8404	0.999	*ωB97XD*
S1 – S3				
χ *vs. A*	1.6338	0.9867	0.948	*B3LYP*
ω *vs. I*	19.407	-3.2091	0.940	*B3LYP*
ω *vs. I*	14.783	-1.9129	0.981	*ωB97XD*

* The significance of the properties is the same as in **Table 8.2**

7.5. Conclusions about properties of azulenes substituted with furan-vinyl-pyridine and thiophene-vinyl-pyridine from quantum mechanics computations

Quantum chemical calculations for azulenes substituted with thiophen– or furan– vinyl– pyridine showed that the predicted chemical parameters are correlated with the experimental electrochemical potentials. Linear relationships with the electron affinity (*A*) or ionization potential (*I*) were considered for the predicted molecular, QSAR properties, and quantum chemical reactivity parameters. For oxygen compounds, the dependencies of the molecular and QSAR properties with *I* (calculated with *ωB97XD* hybrid functional) are linear (R 2 > 0.9), except for PSA and *Epot*, which are better correlated with *A*. For sulfur compounds, the best correlations were obtained with I, most of them by using the *B3LYP* method. For oxygen compounds, the dependencies of the quantum chemical reactivity parameters indicate better correlations of η, σ, and ω with *I* than with *A*, while the correlation χ (*A*) is better than χ (*I*). For sulfur compounds, good correlations were found only for χ (*A*) and ω (*I*), when using the *B3LYP* method.

The energies of the HOMO orbital follow the same order as the experimental values of the first anodic peak potentials. The same result was observed for the first cathodic peak potentials, which vary in the opposite direction, as expected. The redox potential is influenced by the number and position of the alkyl groups. Linear dependencies of DFT-computed energies of FMOs and the experimental oxidation and reduction potentials were found. This computational study proves to be a good alternative approach to determine valuable parameters if we want to assess whether a certain ligand is good for a certain application. Both used density hybrid functionals give reliable results for properties computations and correlations and, therefore, are useful tools to further assess electrochemical applications. Thus, it is challenging to choose the preferred calculation hybrid functional.

Selective bibliographic references Chapter 7
[27] **A.-A. Vasile,** E.-M. Ungureanu, G. Stanciu, M. Cristea, A. Stefaniu, Evaluation of (Z)-5-(Azulen-1-ylmethylene)-2-thioxothiazolidin-4-ones Properties Using Quantum Mechanical Calculations, Symmetry, 2021, 13, 1462.
[39] **A.-A. Vasile (Corbei)**, A. Ștefaniu, O. Matica, E.-M. Ungureanu, Quantum reactivity parameters computation for electrochemical behavior assessment, International online symposium "The environment and the industry E-SIMI 2020", 24-25 Septembrie 2020, Poster.
[40] **A.-A. Vasile (Corbei),** G. Stanciu, E.-M. Ungureanu, A. Stefaniu, Global reactivity analysis from quantum parameters on 2,6-bis-(E)-2-(furan-2yl)-4-(4,6,8-trimethylazulen-1yl)pyridine structure, IX

International Scientific Conference "Actual Problems of Solid State Physics", 22-26 noiembrie 2021, Minsk, Belarus, Poster Theor21.

CONCLUSIONS
C1. GENERAL CONCLUSIONS

In this doctoral thesis, research was conducted on the evaluation of the properties of azulene derivatives in quantum mechanics calculations in order to characterize new organic compounds for different applications, mainly for obtaining chemically modified electrodes for the analysis of mineral or organic species and for creation and design of new optimized analogues that have potential applications in the medical and pharmaceutical field, for subsequent preclinical tests.

The original research was aimed at evaluating the properties that the studied compounds must meet in order to be used in chemical and pharmaceutical engineering applications. In **Chapter 1**, a review was made of the fields of application of chemoinformatics tools, theoretical models and the most important parameters that are necessary for a virtual screening. The potential applications of virtual screening are in the medical field, namely for the design of anticancer therapy, for the treatment of diseases such as Parkinson's and Alzheimer's, for the design of antimicrobial agents, for the identification and quantification of substances of abuse and last but not least. heavy.

Chapter 2 addressed the subject of molecular docking as a tool in the rational design of drugs and explained the steps taken to perform docking, namely ligand preparation, receptor preparation and binding site identification, establishing ligands used for docking, docking protocol validation and analysis of the results obtained.

Chapter 3 reviewed molecular descriptors used to evaluate the properties of organic molecules, materials, and methods used to calculate predictive properties for three well-known pharmacological compounds, namely linezolid, ciprofloxacin, and cadazolid. These ligands were used to perform the docking on the protein of the ribosomal subunit Staphylococcus aureus, with ID in Protein Data Bank: *4WFA*. The naturally occurring ligand (co-crystallized linezolid) on the target protein was extracted and re-docked to validate the docking process, after which each of the three selected ligands was docked. The result obtained from the process of simulating the molecular docking of these three ligands to the target protein is relevant for this paper because it is a study of pharmacological compounds whose antimicrobial activity is known and provides important information about the steps to be taken to complete the process. molecular docking and interpretation of predicted data.

Chapter 4 contains the calculation details for the preliminary characterization and evaluation of the potential of 1,3,4-thiadiazoles to be candidates as drugs. This chapter provides details on the evaluation of the properties of some azulene derivatives: 1,3,4-thiadiazoles, (Z)-5-(azulen-1-ylmethylene)-2-thioxothiazolidin-4-one, thiophene-substituted azulenes, or furan-vinyl-pyridine.

Chapter 5 contains the results of calculations on *in silico* characterization and preliminary evaluation of some 1,3,4-azulene thiadiazoles, docking studies performed on some 1,3,4-thiadiazoles azulene, molecular docking protocol for 1,3,4-thiadiazoles , molecular docking simulations for native ligand and synthesized ligands: 2-phenyl-5- ((4,6,8-trimethylazulen-1-yl) diazenyl) -1,3,4-thiadiazole (**T1**), 2- (azulene -1-yl) -5-phenyl-1,3,4-thiadiazole (**T2**) and 2- (azulen-1-yldiazenyl) -5- (thiophen-2-yl)-1,3,4-thiadiazole (**T3**)), conclusions on docking simulations for native ligand and **T1-T3** ligands, calculations of quantum mechanics on 1,3,4-thiadiazole derivatives with electrochemical applications: 2- (azulen-1-yldiazenyl) -5- (methylsulfonyl) -1,3,4-thiadiazole (**T4**) and 2- (azulen-1-yldiazenyl)-5- (methylsulfinyl) -1,3,4-thiadiazole (**T5**).

In **Chapter 6**, the properties of (Z)-5- (azulen-1-ylmethylene)-2-thioxothiazolidin-4-one were evaluated using quantum mechanical calculations. The original results obtained refer to properties calculated for NMR chemical shifts (which were compared to experimental ones) and molecular and QSAR properties. Correlations were made between the energies of the frontier molecular orbitals calculated by DFT and the experimental data by making predictions of NMR and molecular properties and QSAR. Results were obtained by using two functional models: *B3LYP* and *ωB97XD* to highlight

the variation of properties between the investigated structures. The correlation of molecular properties and QSAR and the correlation of quantum chemical reactivity parameters were performed, as well as the correlations between the energies of the molecular frontier orbitals calculated by DFT and the oxidation and reduction potentials. The predicted chemical parameters were correlated with the experimental electrochemical characterization, in order to establish the best parameters for a ligand to be used for the complexation of heavy metal ions (HMs). The results of the evaluation of the oxidation capacity of the investigated azulene systems were in good agreement with the previously reported electrochemical data.

Chapter 7 presents results on the evaluation of properties by quantum mechanical calculations for azulene substituted with thiophene- or furan-vinyl-pyridine. Calculation details for thiophen- or furan-vinyl-pyridine substituted azulenes are given: 2,6-bis ((E)-2-(thiophen-2-yl) vinyl) -4-(5-isopropyl-3,8 -dimethylazulen-1-yl) pyridine (**S1**) and 2,5-bis ((E)-2-(furan-2-yl) vinyl)-4- (4,6,8-trimethylaz-len-1-yl) pyridine (**O2**). The study of thiophen- or furan-vinyl-pyridine-substituted azulene properties allowed the calculation of molecular properties and QSAR and the correlation between the energies of frontier molecular orbitals by DFT and experimental data, the correlations between molecular properties and QSAR and ionization potential (*I*) or respectively the electronic affinity (*A*), the correlation of the quantum chemical reactivity parameters. Quantum chemical calculations for three-ligand derivatives of (Z) -5- (azulen-1-ylmethylene) -2-thioxothiazolidin-4-one which are structurally distinct by substituting the azulene ring and the methyl and isopropyl groups, respectively: 3 , 8-Me$_2$-5-iPr (**T1**), 4,6,8-Me$_3$ (**T2**) and H (**T3**) resulted in a number of atomic descriptors (bond lengths, angles, Mulliken charges) and particularly molecular valuable in the analysis of quantitative relationships structure-activity and NMR spectra. These predicted chemical parameters were correlated with experimental electrochemical data to determine the best parameters for a ligand to be used for HMs ion complexation. The results of the evaluation of the oxidation capacity of the investigated azulene systems proved to be in good agreement with the previously reported electrochemical data. Linear correlations of the energies of the frontier molecular orbitals calculated by DFT and the experimental oxidation and reduction potentials were found. The computer-aided study has proven to be an alternative to finding the parameters that matter when designing new ligands.

C2. PERSONAL CONTRIBUTIONS

This thesis interconnects the medical field, the pharmaceutical field and chemical engineering, by performing correlations of research data in organic and inorganic chemistry, electrochemistry, biology and biochemistry and is supported by a large volume of studies through modern analysis techniques. The calculations and correlations made led to the following original contributions:

- Quantum mechanics calculations using Functional Density Theory (DFT) for azulene derivatives ((Z)-5-((5-isopropyl-3,8-dimethylazulen-1-yl) methylene)-2-thioxothiazolidin-4-one (**T1**), (Z)-5-((4,6,8-trimethylazulen-1-yl)methylene)-2-thioxothiazolidin-4-one (**T2**), (Z)-5-[(azulen-1-ylmethylene)]-2-thioxothiazolidin-4-one(**T3**),2-(azulen-1-yldiazenyl)-5-(methylsulfonyl)-1,3,4-thia-diazole (**T4**), 2-(azulen-1-yldiazenyl)-5-(methylsulfonyl)-1,3,4-thiadiazoles (**T5**)) and the correlation of the data obtained with the existing data in the literature, thus proving that the computer-assisted study is a complex structural approach and an alternative method of finding the parameters of interest for design of new ligands;

- Evaluation of properties resulting from quantum mechanics calculations for thiophen substituted azulene (2,6-bis((E)-2-(thiophen-2-yl)vinyl)-4-(5-isopropyl-3,8-dimethylazulene)-1-yl) pyridine (**S1**), 2,6-bis((E)-2-(thiophen-2-yl)vinyl)-4-(4,6,8-trimethylazulen-1-yl) pyridine (**S2**)), 4-(azulen-1-yl)-2,6-bis ((E)-2-(thiophen-2-yl)vinyl)pyridine (**S3**) or furan-vinyl-pyridine (2,6-bis((E)-2-(furan-2-yl)vinyl)-4-(5-isopropyl-3,8-dimethylazulen-1-yl) (**O1**), 2,6-bis ((E)-2-(furan-2-yl)vinyl) -4-(4,6,8-trimethylazulen-1-yl) (**O2**), 4-(azulen-1-yl)-2,6-bis((E)-2-(furan-2-yl) vinyl) pyridine (**O3**)) and

the correlation of the predicted chemical parameters with the experimental electrochemical potentials, thus proving that computational study is an approach to find suitable ligands for certain applications;

- *In silico* characterization and preliminary anticancer evaluation of 1,3,4-thiadiazoles: 2-phenyl-5-((4,6,8-trimethylazulen-1-yl) diazenyl) -1,3,4-thiadiazole (**T1**), 2-(azulen-1-yl) diazenyl) -5-phenyl-1,3,4-thiadiazole (**T2**), 2-(azulen-1-yl)diazenyl) -5- (thiophen-2-yl) -1,3,4-Thiadiazole (**T3**) compounds that can be used to make drugs with antiproliferative potential.

C3. FUTURE DEVELOPMENT PROSPECTS

Through the computational studies performed, the present doctoral thesis opens perspectives regarding:

- Alternative approaches valid to determine valuable parameters to assess whether a particular ligand is good for a particular application. Both functional density hybrids used provide reliable results for properties and correlation calculations and are useful tools for further evaluation of electrochemical applications;

- Evaluation of properties for new azulene organic compounds and design of optimized hybrid structural analogues with potential applications in the medical and pharmaceutical field, for further preclinical tests;

- Characterization of new organic compounds and their evaluation for various applications, mainly for the production of chemically modified electrodes for the analysis of mineral or organic species;

- Design of new ligands to obtain complexing electrodes for the detection of analytical targets of environmental interest.